RESOLUTION OF SUB-SEISMIC RESERVOIRS BY THE APPLICATION OF SPECTRAL DECOMPOSITION AND SPECTRAL INVERSION METHODS IN BOONSVILLE FIELD, NORTH CENTRAL TEXAS

An Abstract of a Thesis

Presented to

the Faculty of the Department of Earth and Atmospheric Sciences

University of Houston

In Partial Fulfillment

of the Requirements for the Degree

Master of Science

By

Ayodeji Babalola

May, 2013

RESOLUTION OF SUB-SEISMIC RESERVOIRS BY THE APPLICATION OF SPECTRAL DECOMPOSITION AND SPECTRAL INVERSION METHODS IN BOONSVILLE FIELD, NORTH CENTRAL TEXAS

………………………………...

Ayodeji Babalola

APPROVED:

………………………………...

Dr. John Castagna,

Chairman

………………………………...

Dr. Evgeni Chesnokov,

Member

………………………………...

Dr. Marianne Rauch-Davies,

Member

………………………………

Dean, College of Natural
Sciences and Mathematics

ACKNOWLEDMENT

My special thanks go to God Almighty for his provision, gift of life, and strength during the course of my study. I am thankful and indebted to many people and institutions, which have made possible this thesis and my graduate studies. I would like to personally thank to my advisor, Dr. John Castagna for his guidance, support and the confidence he has given me throughout this research.

I really appreciate the assistance given to me by Dr. Marianne-Rauch Davies and Dr. Evgeni Chesnokov for their technical support, guidance, and encouragements. I would specially like to acknowledge the professors and the staff of the geophysics faculty for their commitment to the success of the students.

I really appreciate all the members of my family: my parents, Dr. M.T and Mrs. Babalola, whom I dedicate this thesis to, and my siblings, Olaitan, Olalekan, Oludolapo, Afolabi and Olufisayo for their financial and moral support during the period of my study at the University of Houston. I am very grateful for the help rendered by Dr. Charles Puryear, Arnold Oyem, Dr. Sunday Amoyedo, Debo Adekunle, Oyedoyin Oyetunji, and Bode Omoboya during the period of this research .

RESOLUTION OF SUB-SEISMIC RESERVOIRS BY THE APPLICATION OF SPECTRAL DECOMPOSITION AND SPECTRAL INVERSION METHODS IN BOONSVILLE FIELD, NORTH CENTRAL TEXAS

An Abstract of a Thesis

Presented to

the Faculty of the Department of Earth and Atmospheric Sciences

University of Houston

In Partial Fulfillment

of the Requirements for the Degree

Master of Science

By

Ayodeji Babalola

May, 2013

ABSTRACT

Constrained least squares-spectral analysis (CLSSA) and high resolution spectral inversion are applied to 3D seismic dataset from Boonsville field to overcome the wavelet interference arising from complex reflection patterns created by thin layering within Atoka conglomerate that forms the producing unit in this field. The Atokan conglomerate is a case of thin bed reservoir with discontinuous beds that depict seismic resolution below the typical Widess limit, making bed thickness estimation using conventional means almost impossible.

Apparent bed thickness estimates are obtained from analyzing high resolution spectral inversion attribute volumes and the result compared with true bed thickness estimated from stratigraphic correlation of well log data. The results are found to be highly correlated, showing a great improvement in the temporal resolution from the high resolution volume. The inverted data furthermore revealed several minor faults and also enhances lateral bed continuity that were initially interpreted discontinuous due to wavelet distortion on seismic. These comparative analyses clearly show that spectral analysis using CLSSA and spectral inversion give temporal resolutions that are not achievable using the conventional Widess theory.

TABLE OF CONTENT

LIST OF FIGURES

CHAPTER 1

INTRODUCTION

1.1 BACKGROUND

The main purpose of this research is to apply spectral decomposition and spectral inversion techniques to resolve beds that are below seismic resolution in Boonsville field. Vertical seismic resolution is defined as the ability to separate or distinguish between two or more close events (reflections) in the time/depth domain (Chopra et al., 2006a). Conventional thickness estimation workflow (Widess theory) restrict the limit of vertical seismic resolution to ¼ of the seismic wavelength, this has imposed a level of uncertainty in estimating important parameters (net-gross, lithology) in reservoir models and also underestimates reservoirs by bypassing pay zones.

Thin layers within a formation creates complex reflection patterns caused by interferences of two closely spaced events, the tuning effects within a formation consequently affect seismic amplitude and restrict the ability to vertically separate these events. Boonsville field, located in North Central Texas is underlain by Paleozoic carbonates: the clastic section within the dataset is related to the Atoka conglomerate which is deposited in the fluvial-deltaic environment and is thin and discontinuous reservoirs. Typical seismic signature of these high-impedance sands is a peak-trough but the layers are so thin, less than 40ft (12.1m) that seismic could not adequately distinguish the top from the base. Spectral analysis (spectral decomposition and inversion) is carried out to extract these fine details (thickness and stratigraphy) that will better characterize the unit.

Spectral decomposition refers to any method that produces a continuous time-frequency analysis in each time sample of a seismic trace (Castagna and Sun, 2006): the manner in which time series is mapped into the frequency spectrum determines the amount of new information that can be obtained (Chakraborty and Okaya, 1995). The premise behind spectral decomposition as thin-bed analytic tool is that reflections from thin layers have a unique signature in the frequency domain that is indicative of time thickness: the amplitude interference spectrum delineate thin-bed variability via spectral notching patterns while the phase spectrum respond to lateral discontuity via local phase instability (Partyka et al., 1999). The method also aid conventional seismic interpretation by its recent development as an hydrocarbon indicator (Castagna et al., 2003).

Additional detailed information of the subsurface can be extracted from high resolution spectral inversion results: this process removes the effect of wavelet distortion on the reflectivity series thereby allow two closely spaced events in time to be resolved (Puryear and Castagna, 2008).

The research focused on characterizing sub seismic reservoirs in Boonsville field, North Texas by adopting spectral decomposition and inversion methods especially in resolving the discontinuities in the Atoka sand packages and consequent improvement in temporal resolution of the dataset.

1.2 RESEARCH OBJECTIVES

This research applies spectral decomposition and spectral inversion techniques to resolve thin sands within the Boonsville field, the main objectives of this work are listed below:

- The research aim is to compare different spectral decomposition methods to delineate the best algorithm with superior time-frequency resolution that will eventually be used as an input into the inversion algorithm.
- To apply spectral decomposition and inversion techniques to resolving sub-seismic reservoirs in Boonsville field.

1.3 AVAILABLE DATA SET

Boonsville field dataset is made publicly available by the Bureau of Economic Geology (BEG), University of Texas at Austin as a work sponsored by Gas Research Institute (GRI). The dataset contains:

- The 5.5mi^2 (14.24 km^2) of time migrated seismic data with 110ft by 110ft (33.5m by 33.5m) stacking bins, there are 122 lines and 121 traces.
- Digitized well curves from 38 wells inside the 3-D seismic grid.
- Depths to the boundaries of many genetic sequences within the Bend conglomerate interpreted by Bureau of Economic Geology (BEG) from the logs.
- Vertical seismic profiles (VSP) data and explosive-source checkshot data in a calibration well near the center of the seismic grid.

1.4 GEOLOGY OF BOONSVILLE FIELD

Boonsville field is located in Jack and Wise Counties in the Fort Worth Basin in North Central Texas (Fig 1.1) and is one of the largest natural gas producing fields. Figure 1.2 is a generalized Post-Mississippian description of the stratigraphic columns at the Fort Worth Basin. It consists of several formations spanning from the Ellenburger (Ordovocian) to the Strawn (Middle Pennsylvanian), but gas production occurs only at the Atoka Bend Conglomerate which is defined as the interval between the top of the Caddo limestone to the top of the Marble Falls. This zone define the engineering and geological information in the data (Hardage , 1996).

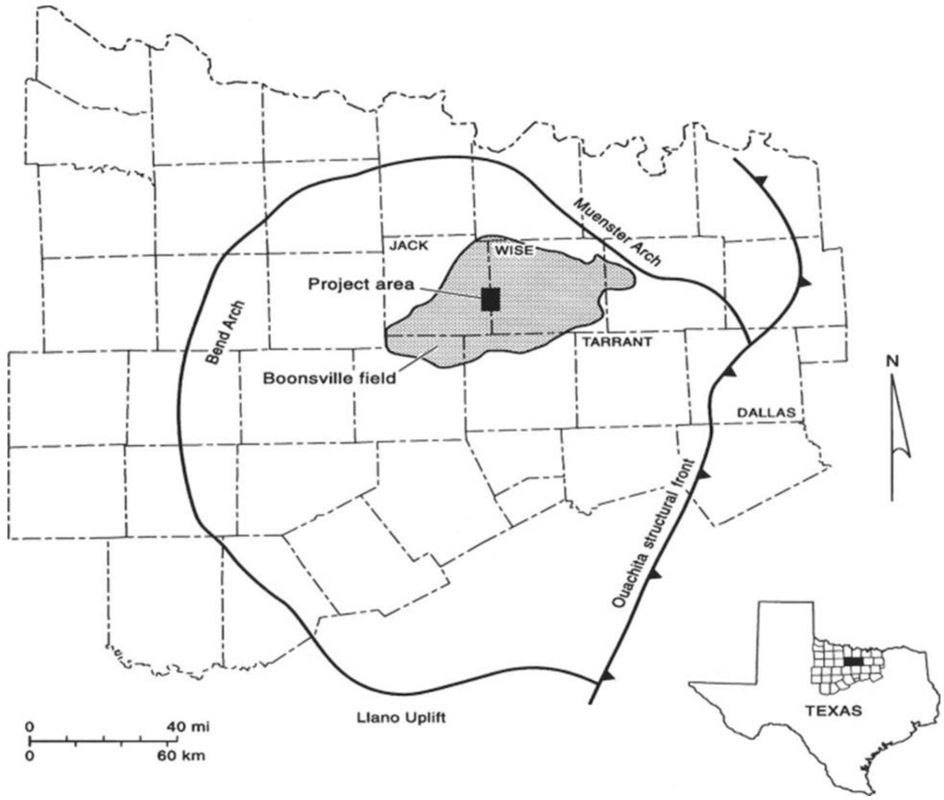

Fig 1.1: Location map of Boonsville field in Jack and Wise Counties in the Fort Worth Basin in North Central Texas (modified from Hardage et al., 1996)

1.4.1 RESERVOIR CHARACTERISTIC

The Atoka Bend conglomerate, deposited in a fluvio-deltaic environment (Thompson, 1982) is a gas producing reservoir with a thickness that ranges from 900-1300ft (275-400m). The sandstone reservoirs are thin and discontinuous and are also underlain by Paleozoic carbonates: the deepest being the Ellenburger Group. Previous work revealed that numerous karst structures occurred in the deep Ellenburger carbonates (Ordovician) and karst-generated collapse created breccia pipes and structural sags that extended upward as high as 2500ft (760m). These structures influence sandstone distribution pattern and reservoir compartmentalization in the Shallower Bend Conglomerate (Hardage et al.,1996).

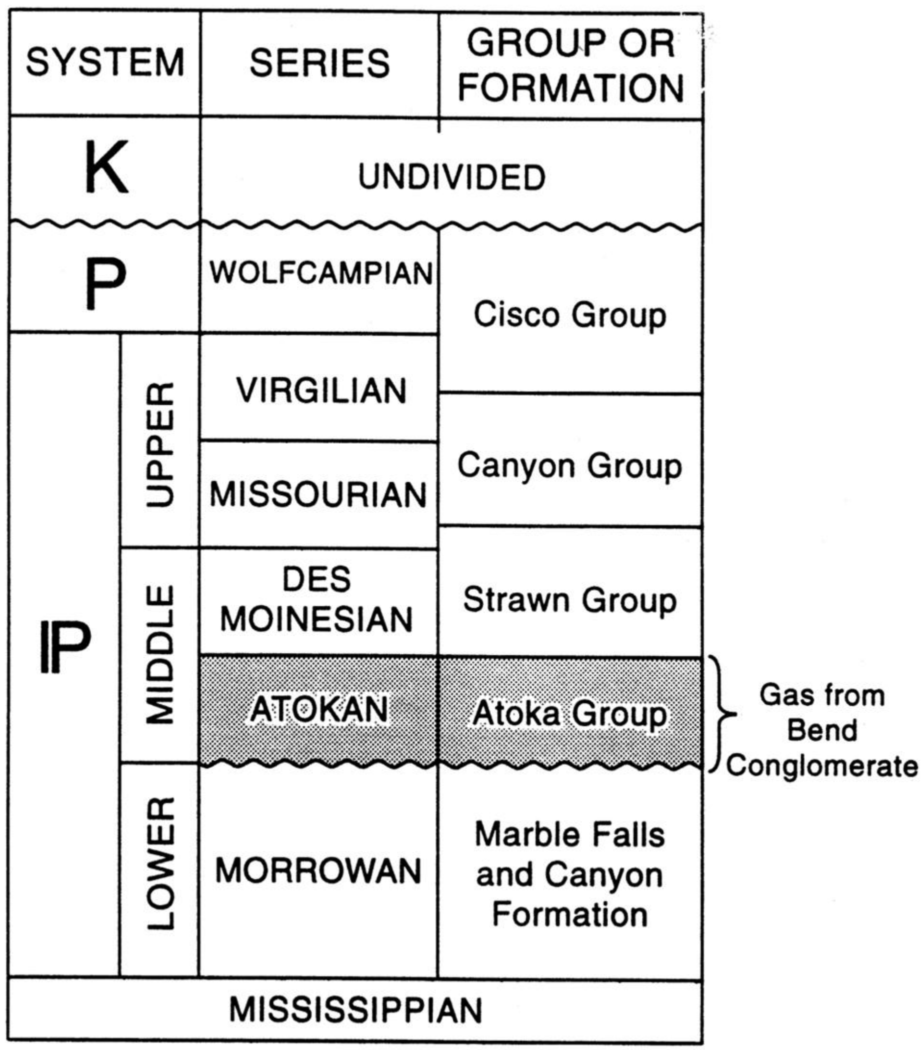

Fig 1.2: Generalized post-Mississippian stratigraphic column for the Fort Worth Basin (modified from Hardage et al., 1996)

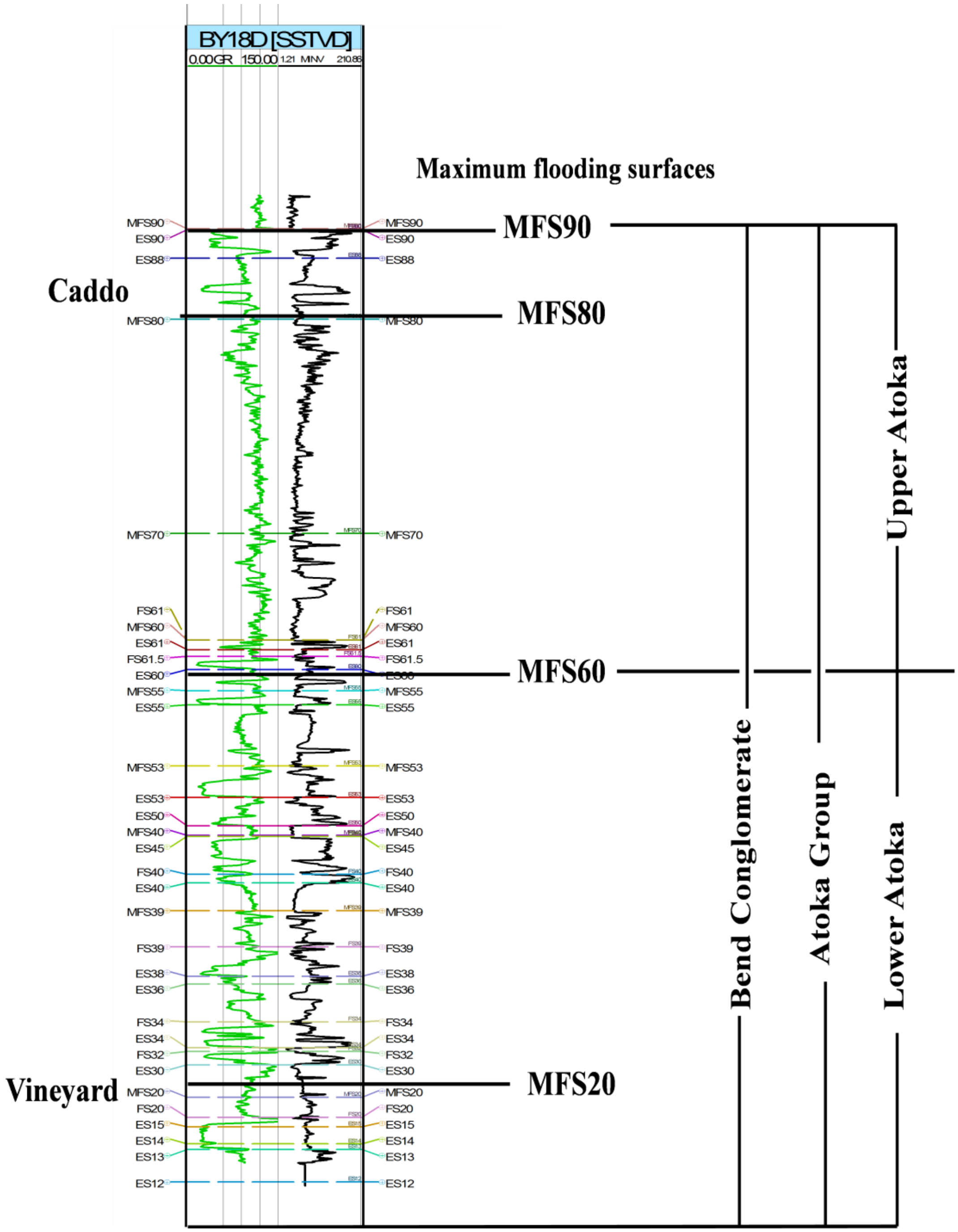

Fig 1.3: Stratigraphic nomenclature used to define Bend Conglomerate genetic sequences in Boonsville field.

1.5 METHODOLOGY

Thin-bed analysis in Boonsville field utilize spectral methods to improve temporal resolution of sand bodies that are below conventional seismic resolution limit, this study is divided into three sub categories :

- 3D Seismic data interpretation and delineation of data resolution limit from modeling by applying conventional means of thickness estimation.
- Thickness estimation from mapping discrete frequency volume.
- Application of spectral inversion technique to remove wavelet destructive interference effect from seismic data and also invert for layer thickness, producing high resolution data that vertically separates events that were originally distorted by wavelet interference.

These results are reconciled to furnish final interpretation for better characterized reservoirs within the field, the workflow is shown below:

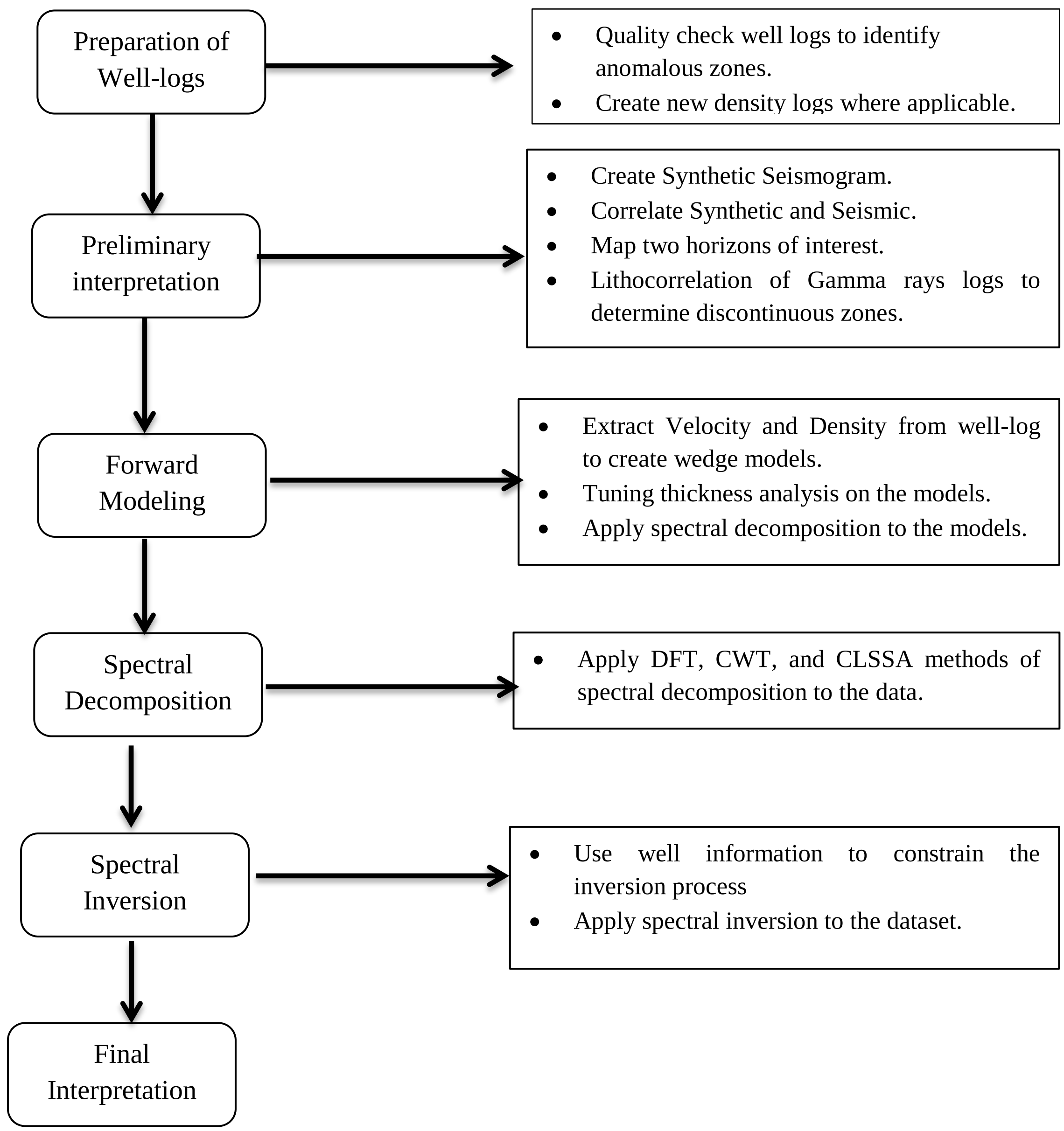

Fig 1.4: Research workflow

CHAPTER 2

3D SEISMIC INTERPRETATION AND MODELING

2.0 INTRODUCTION

In this section, structural and stratigraphic information derived from incorporating seismic and well data in the time domain will be discussed. This is aimed at paving the way for a more detailed work done with spectral analysis. The section commences by the reconciliation of available well and seismic datasets, finally culminating to seismic modeling (wedge models) that establishes the motive for the application of spectral inversion and decomposition for thin-bed study in Boonsville field.

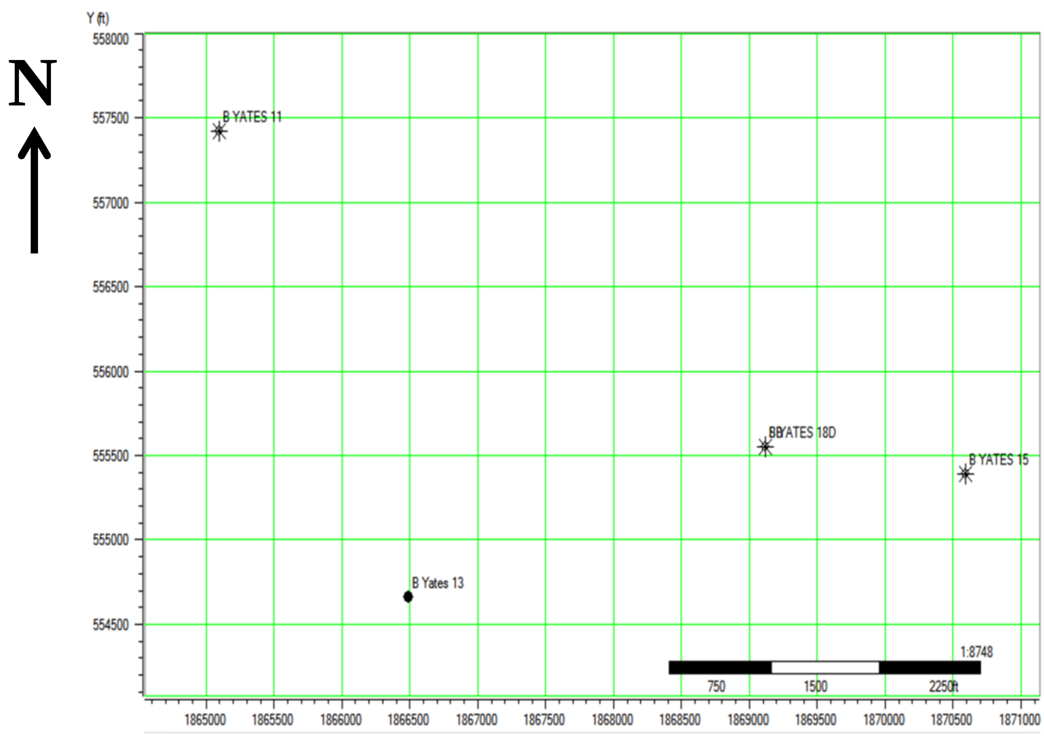

Fig 2.1: Basemap of Boonsville field with well logs

2.1 LITHOCORRELATION

Lithocorrelation is the delineation of stratigraphic information over an area using well-logs: wells are lithocorrelated to discern the continuity of formations across a field. For this work, gamma ray and deep resistivity log were used. Figure 2(a) is a profile cutting across wells (BY11, BY18D, and BY15), while fig 2(b) is second profile along wells BY13, CY9, and BY18D. The tops are interpreted genetic sequences within the Atoka Conglomerate by the Bureau of Economic Geology, University of Texas at Austin. These correlation panels depict several thin sand reservoirs that would be difficult to be interpreted as separate events on seismic.

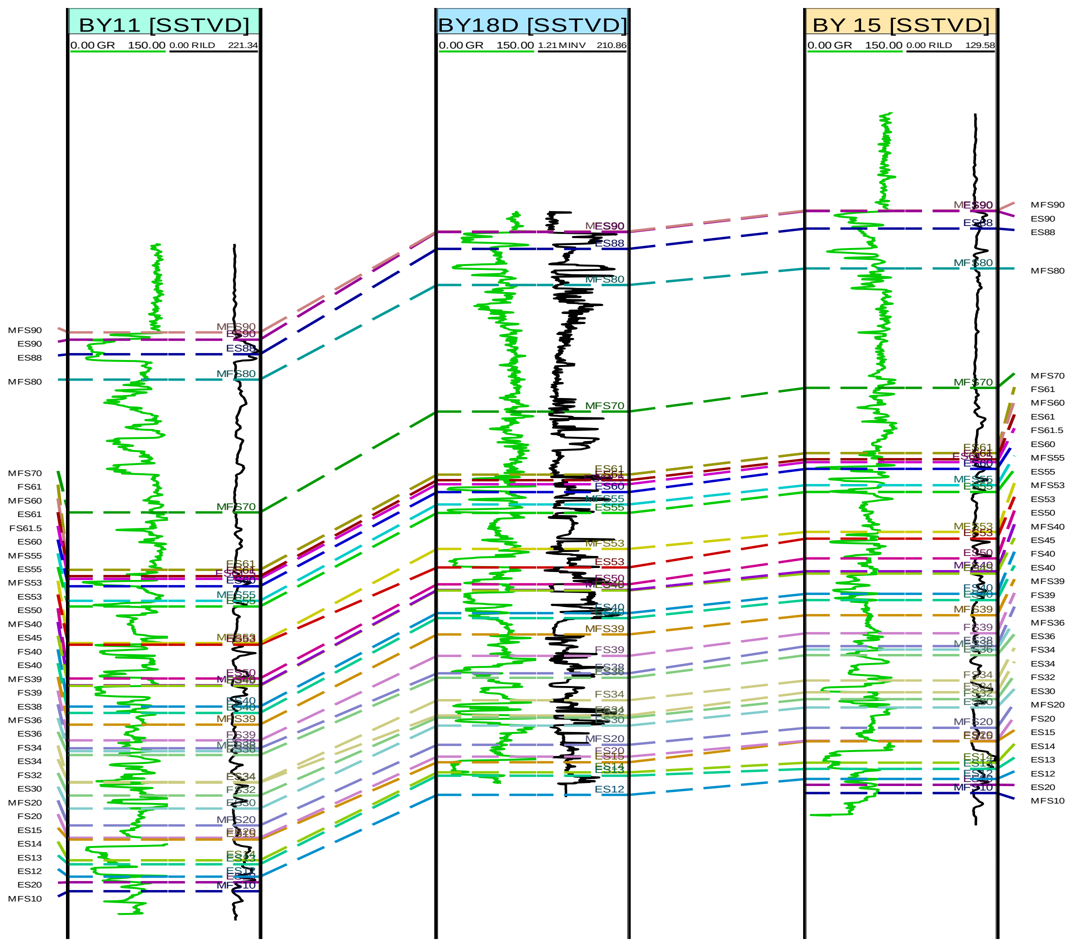

Fig 2.2(a): Correlation panel though wells BY11, BY18D, and BY 15

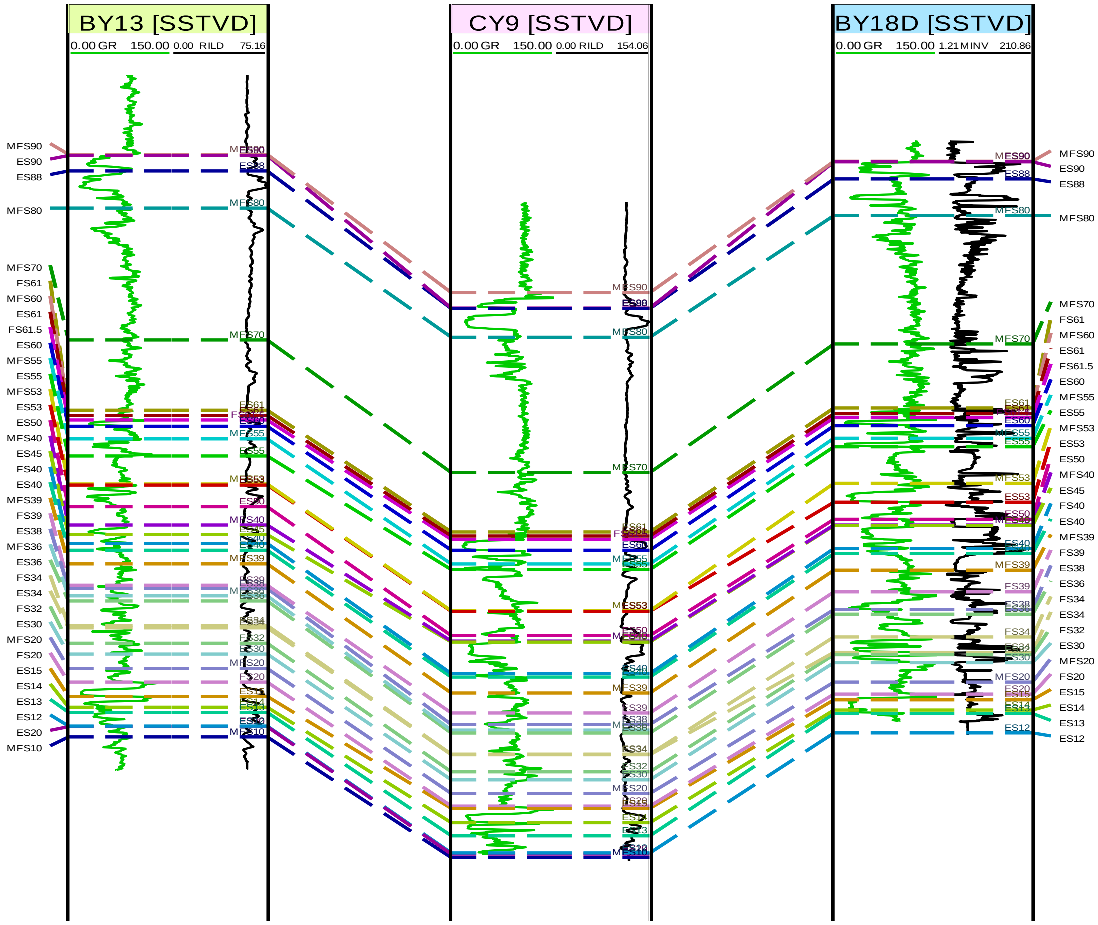

Fig 2.2(b): Correlation panel though wells BY13, CY9, and BY18D

2.2 DISPERSION

One of the problems associated with reconciling well log data and surface seismic is dispersion. Sonic logs are measured in kilohertz scale compared to surface seismic measured in hundredth of Hertz. Because it has a much shorter wavelength, the sonic log signal may be influenced by small scale features in the travel path, such as mineral inclusions. Fractures and bed boundaries also act as discrete discontinuities to the high frequency signal. At the longer wavelength used in surface seismic surveys, all of these features are averaged into the bulk properties of the rock (Liu, 1987; Paillet and Cheng, 1991)

However, seismic respond to lateral facies changes and heterogeneities which are not visible at the well bore scale**.** In the case of normal dispersion, high frequencies travel faster than low frequencies, so that the integrated sonic log travel times are generally shorter than seismic travel times (Stewart et al., 1984). In preparation for adequate seismic-well tie, the different scales of the seismic and well data must be reconciled and this is achieved through the processes of Blocking and Backus-averaging.

2.2.1 WELL-LOG BLOCKING AND BACKUS-AVERAGING

The essence of Blocking and Backus-averaging of well-logs is to solve the dispersive phenomenon and upscale borehole data to seismic scale. Well-log Blocking is the averaging of log data within a certain threshold and replacing the log measurement with the mean value within the block. The result of log Blocking process is a simplified earth model that retains the coarse information in the well-logs but dismisses fine information that is unresolvable in the seismic data (Craig, 1992). Averaged well data still retains significant events in the log that can be correlated to seismic. The non-uniform Blocking algorithm used in the course of this work entails searching the smoothed version of the well-logs for large changes in slopes: searching for extrema in the derivative of the amplitude with respect to depth (Souder and Pickett, 1972).

2.2.2 BACKUS-AVERAGING

Backus-averaging is a form of upscaling in which earth parameters are estimated at frequencies or wavelength far different from those involved in the original measurements (Liner and Tong, 2007). The earth is made of several thin layers that are less than the seismic wavelength Fig (2.3), if these layers are either isotropic or anisotropic (transversely-isotropic), the stack act like an anisotropic medium.

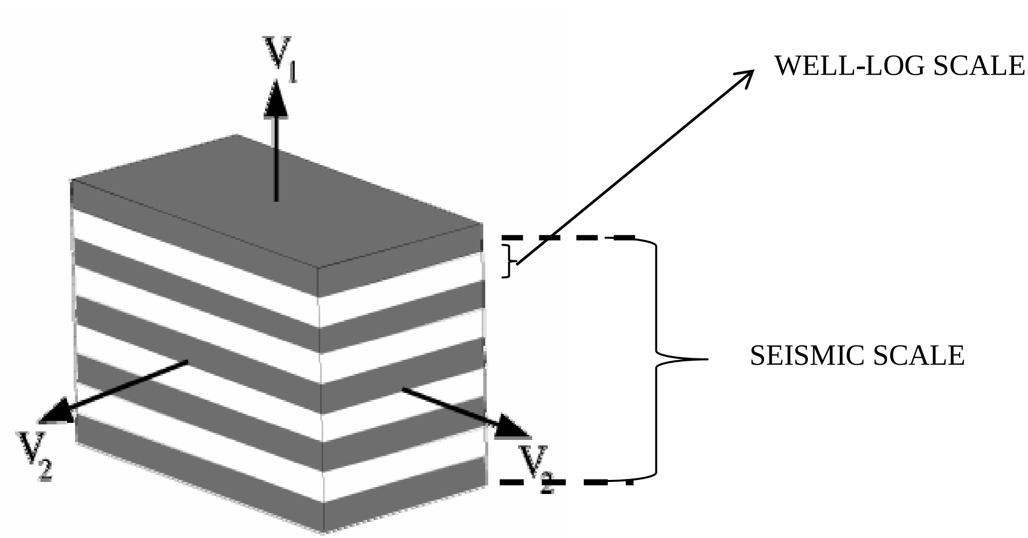

Fig 2.3: Comparison of seismic and well-log scale

The elastic stiffness tensor of a transversely anisotropic medium, symmetric in the x3 direction is defined by five independent elastic constants (a,b,c,d,and f). Backus (1962) showed that in the long wavelength limit, a stratified medium composed of transversely isotropic media is also effectively anisotropic with effective elastic stiffness shown below (Mavko et al., 2009).

Backus-averaging in principle is advocating that there should be a method that calculates the anisotropic parameters of the stratified medium due to any wavelength that passes through the medium.

$$\begin{matrix} a & b & f & 0 & 0 & 0 \\ b & a & f & 0 & 0 & 0 \\ f & f & c & 0 & 0 & 0 \\ 0 & 0 & 0 & d & 0 & 0 \\ 0 & 0 & 0 & 0 & d & 0 \\ 0 & 0 & 0 & 0 & 0 & m \end{matrix} \quad , m = \frac{1}{2}(a-b) \tag{2.1a}$$

The medium described by (A, B, C, D, and F) is the long wavelength equivalent of the original stack of layers and is smoother and generally more anisotropic than the original.

$$\begin{matrix} A & B & F & 0 & 0 & 0 \\ b & A & F & 0 & 0 & 0 \\ F & F & F & 0 & 0 & 0 \\ 0 & 0 & 0 & D & 0 & 0 \\ 0 & 0 & 0 & 0 & D & 0 \\ 0 & 0 & 0 & 0 & 0 & M \end{matrix} \quad , \mathrm{M}= \frac{1}{2}(A-B) \tag{2.2a}$$

$$\mathrm{A} = \langle \mathrm{a} - \mathrm{f}^2\mathrm{c}^{-1}\rangle + \langle \mathrm{c}^{-1}\rangle^{-1}\langle \mathrm{fc}^{-1}\rangle^2 \tag{2.2b}$$

$$\mathrm{B} = \langle \mathrm{b} - \mathrm{f}^2\mathrm{c}^{-1}\rangle + \langle \mathrm{c}^{-1}\rangle^{-1}\langle \mathrm{fc}^{-1}\rangle^2 \tag{2.2c}$$

$$\mathrm{C} = \langle \mathrm{c}^{-1}\rangle^{-1} \tag{2.2d}$$

$$\mathrm{F} = \langle \mathrm{c}^{-1}\rangle^{-1}\langle \mathrm{fc}^{-1}\rangle^2 \tag{2.2e}$$

$$\mathrm{D} = \langle \mathrm{d}^{-1}\rangle^{-1} \tag{2.2f}$$

$$\mathrm{M} = \langle \mathrm{m}\rangle \tag{2.2g}$$

The VTI medium is defined by five(5) independent elastic constants, in the case where the individual layers are isotropic , the number of independent constants required to define each layer will be reduced to two and effective medium will still be anisotropic (transversely isotropic) Substituting equation (2.3) into equations (2.2a-2.2d).

$$a = c+2\mu,\ b= f=\lambda,\ \text{and}\ d=m=\mu \tag{2.3}$$

These equations (2.2a-2.2d) can be rewritten in terms of elastic parameters as (2.4a -2.4f):

$$A = \left\langle\frac{4\mu(\lambda,+\mu)}{\lambda+2\mu}\right\rangle + \left\langle\frac{1}{\lambda+2\mu}\right\rangle^{-1}\left\langle\frac{\lambda}{\lambda+2\mu}\right\rangle^{2} \tag{2.4a}$$

$$B = \left\langle\frac{2\mu\lambda,}{\lambda+2\mu}\right\rangle + \left\langle\frac{1}{\lambda+2\mu}\right\rangle^{-1}\left\langle\frac{\lambda}{\lambda+2\mu}\right\rangle^{2} \tag{2.4b}$$

$$C = \left\langle\frac{1}{\lambda+2\mu}\right\rangle^{-1} \tag{2.4c}$$

$$F = \left\langle\frac{1}{\lambda+2\mu}\right\rangle^{-1}\left\langle\frac{\lambda}{\lambda+2\mu}\right\rangle \tag{2.4d}$$

$$D = \left\langle\frac{1}{\mu}\right\rangle^{-1} \tag{2.4e}$$

$$M = \langle\mu\rangle \tag{2.4f}$$

Since the derived coefficients are VTI stiffness, they can be inverted for wavespeeds, Levin (1979) derived P, S velocities and densities in the isotropic layers from elastic parameters.

$$a = \rho V_p^2,\ d = \rho V_s^2,\ f = (V_p^2 - V_s^2) \tag{2.5}$$

From equation (2.4), In terms of compressional and shear wave velocities, the effective medium parameters can be rewritten as:

$$A = \langle 4\rho V_s^2 \left[1 - \frac{V_s^2}{V_p^2}\right]\rangle + \langle 1 - 2\frac{V_s^2}{V_p^2}\rangle^2 \langle \left(\rho V_p^2\right)^{-1}\rangle^{-1} \tag{2.6a}$$

$$B = \langle 2\rho V_s^2 \left[1 - \frac{2V_s^2}{V_p^2}\right]\rangle + \langle 1 - 2\frac{V_s^2}{V_p^2}\rangle^2 \langle \left(\rho V_p^2\right)^{-1}\rangle^{-1} \tag{2.6b}$$

$$C = \langle \left(\rho V_p^2\right)^{-1}\rangle^{-1} \tag{2.6c}$$

$$F = \langle 1 - 2\frac{V_s^2}{V_p^2}\rangle^2 \langle \left(\rho V_p^2\right)^{-1}\rangle^{-1} \tag{2.7d}$$

$$D = \langle (\rho V_s^2)^{-1}\rangle^{-1} \tag{2.8e}$$

$$C = \langle \rho V_s^2\rangle \tag{2.9f}$$

The long-wavelength anisotropic medium has both the horizontal and vertical components but only the vertical is needed for this work as represented below:

$$V_{p,v} = \sqrt{\frac{C}{\rho}} \text{ and } V_{s,v} = \sqrt{\frac{D}{\rho}} \tag{2.4}$$

Backus–averaging is usually considered a way of smoothing velocity data from wells. Indeed the upscaled vertical P-waves is one product but the theory actually provides a set of VTI parameters (Liner and Tong, 2007). Figure (2.4a) is a plot of original log and Blocked log prior to applying the Backus-averaging algorithm while fig (2.4b) is the final product of log-upscaling process by Blocking and Backus-averaging.

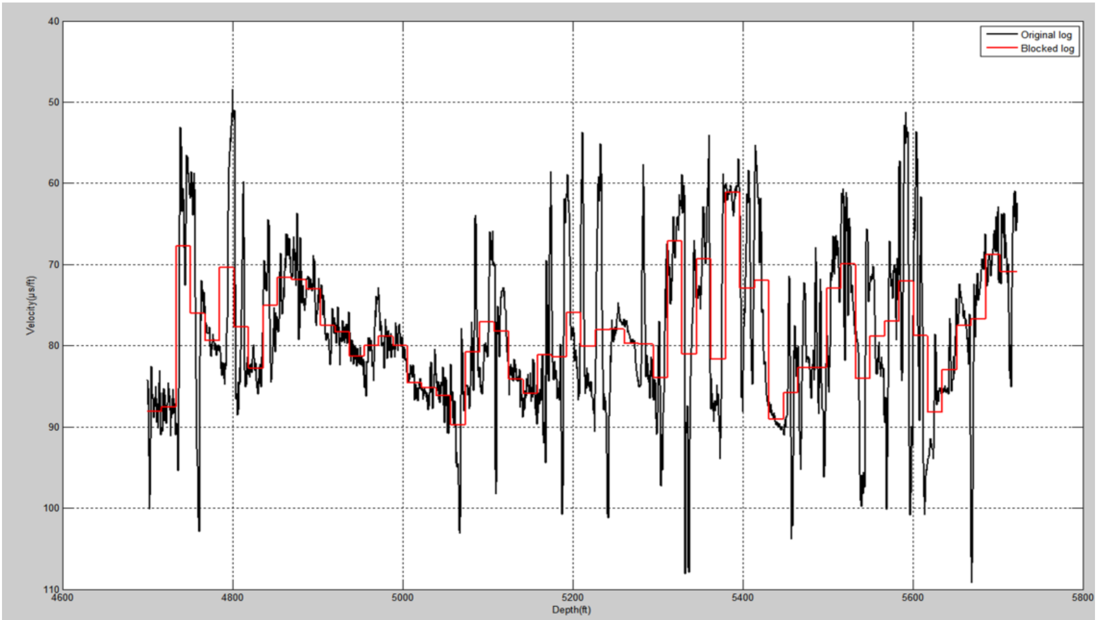

Fig 2.4(a): Blocked log before Backus-averaging

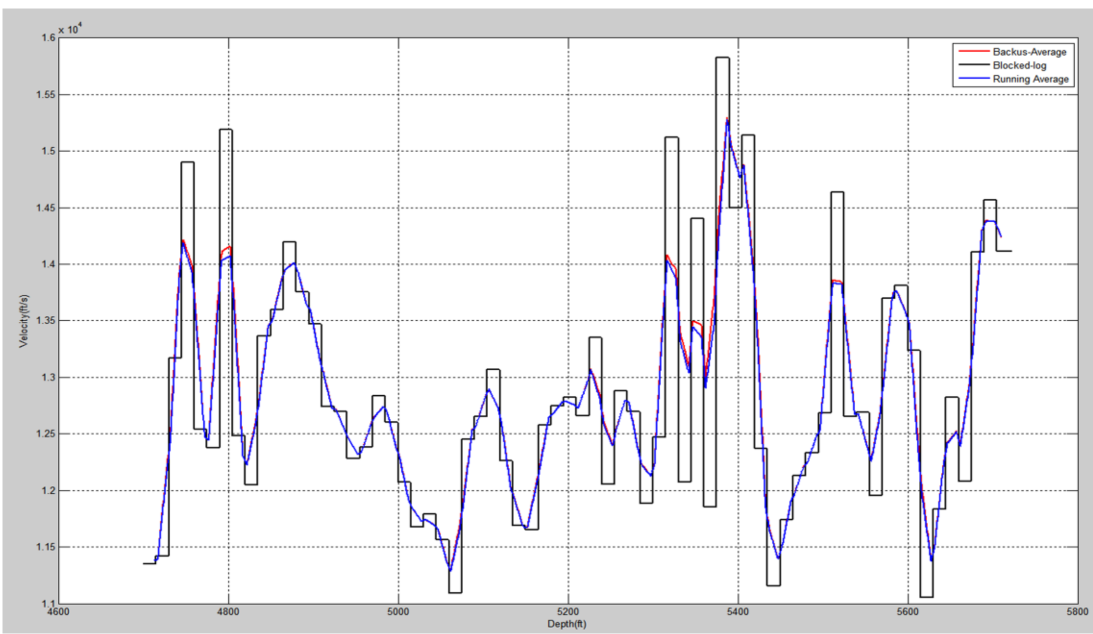

Fig 2.4(b): Blocked log after Backus -averaging

2.2.3 SEISMIIC TO WELL - TIE PROCESS

Prior to upscaling log data, a necessary step is to quality-checked the logs: especially sonic and density logs in readiness for creating synthetic seismograms. Such quality control practices includes despiking, inspecting the caliper for bad data due to invasive / wash-out zones etc. Synthetic seismograms are created by incorporating well-bore data (depth domain) with surface seismic (time domain) such that accurate tops and base of reservoirs from wells can be established with confidence on the seismic.

Even though, there are thirty-four (34) wells in the field, only four (CY9, BY18D, BY11, and BY15) have sonic and density logs while only two (BY18D and CY9) out of the four wells are within the seismic survey. Since Boonsville field is an onshore dataset with surface reference datum of 900ft (274m), one should be careful to make reasonable assumption on the replacement velocity with respect to the underlain stratigraphy (clastic section underlain by a carbonate basement), I used a replacement velocity of 4000m/s.

Generation of synthetic seismograms entails the convolutional operation of a wavelet extracted from the seismic at zones close the coordinates of the well with the reflectivity series, equation (2.5). Statistical wavelet is initially used to align the reflections on the synthetics to the composite trace taking into account other geological data (tops, markers, etc.). A wavelet that is more representative of the amplitude and phase spectrum of the dataset at the well location can be extracted from log since the seismic data has been zero-phased, statistical wavelet was used in the well-tie process. The algorithm for extracting wavelet from log in Hampson-Russell software uses a time-domain operator that shapes the well-log reflectivity to the seismic composite trace to determine the wavelet's amplitude and phase spectra.

$$S(t) = r(t) * w(t) + \text{noise} \qquad (2.5)$$

These wells are tied to seismic by aligning only primary reflections and utilizing only the acoustic waves scenario. Several effects of seismic wave propagation like multiples, attenuation, anisotropy, absorption etc. are also not modeled into the seismic-well tie process since these effects are negligible. Often times, a simple scenario as used in this work is adequate for practical purposes.

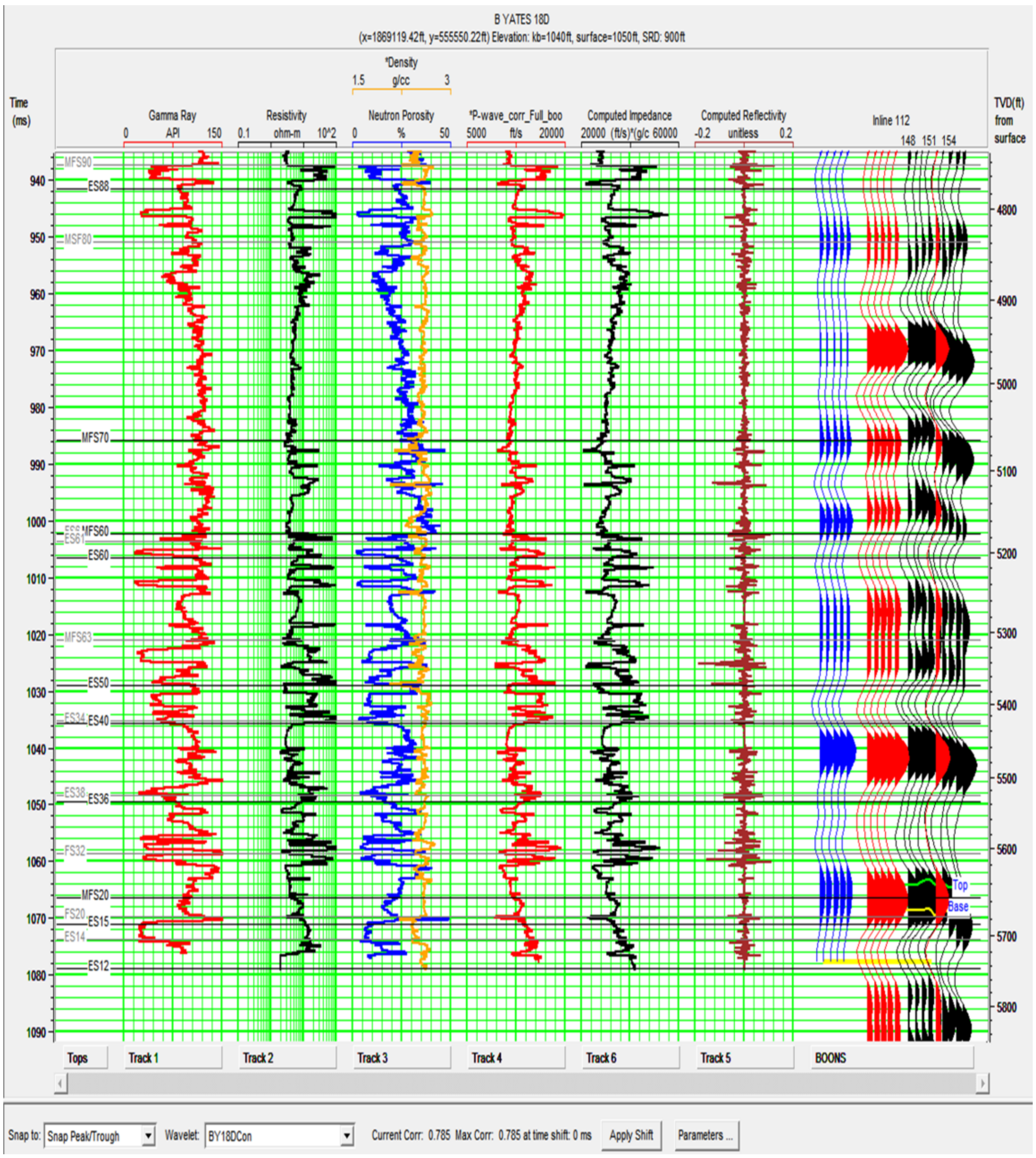

Fig 2. 5: Seismic well-tie using BY18D well (Correlation coefficient is 0.785)

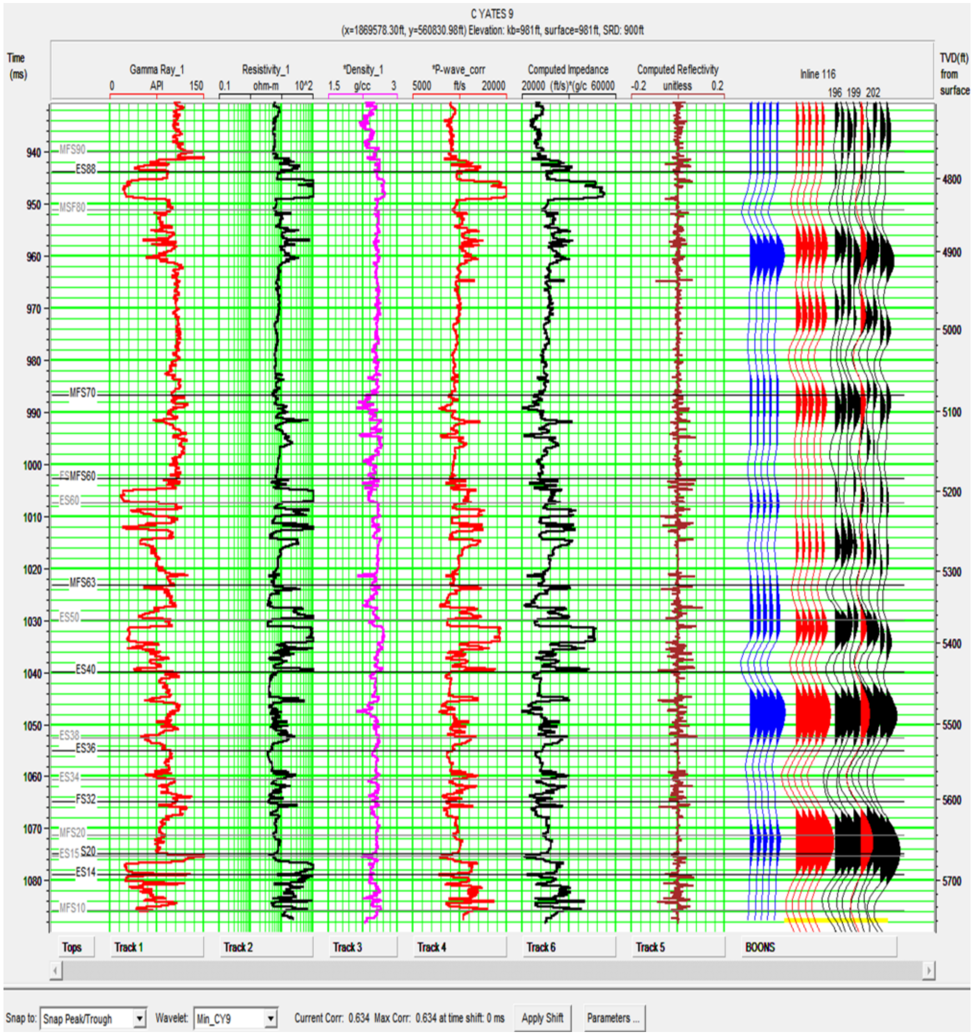

Statistical wavelet (frequency)

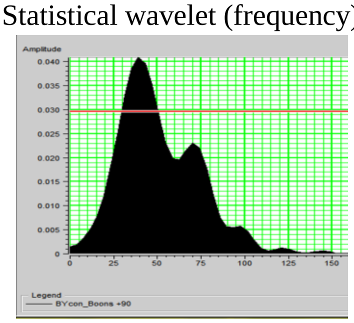

Statistical wavelet (time)

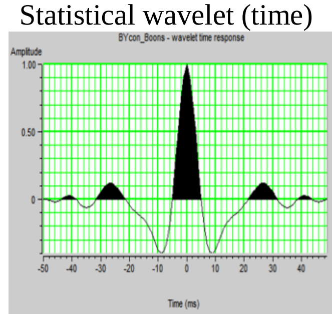

Fig 2. 6: Seismic well-tie using CY9 well (Correlation coefficient is 0.634)

These synthetic are adequately stretched and squeezed taking into account the drift correction (changes in interval velocity during the stretching and squeezing) to properly align the events . Well BY18D's correlation coefficient is 0.785 (fig 2.5) and CY9 is 0.634 (fig 2.6). Final result of the well-tie process is the generation of new depth-time data pairs and well synthetics that properly position the events on seismic.

2.3 HORIZON INTERPRETATION

The product of a good seismic-well tie is the accurate alignment of synthetic seismogram generated from well data with appropriate events on seismic. The top of the clastic section, Caddo (MFS20) was mapped at a seismic time of 940ms and the base, Vineyard (MFS90) is tracked at 1065ms using well BY18D tie. Fig (2.7) is an arbitrary line taken across the two tied wells (CY9 and BY18D) showing the mapped Caddo and Vineyard horizons.

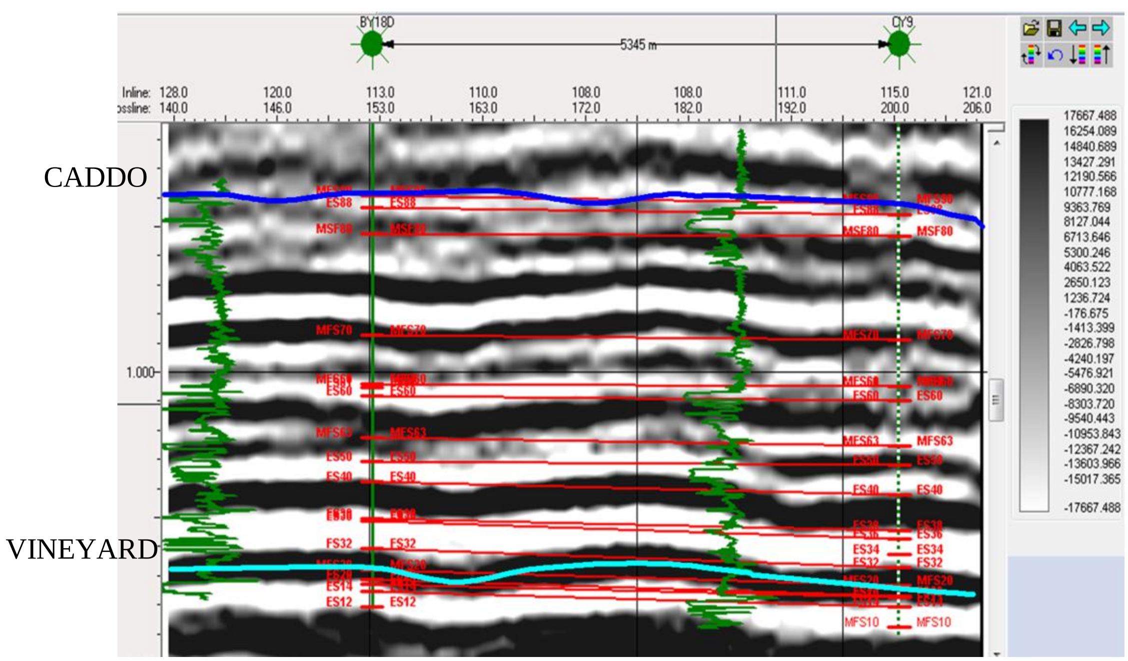

Fig 2.7: Vertical seismic section showing Mapped Vineyard (green) and Caddo Horizons (blue)

3.1 TIME STRUCTURE MAPS

The two events (Vineyards and Caddo) were picked throughout the volume to generate time-structure maps, they are fairly continuous since the field has only few minor faults but predominantly dominated structurally by karst structures. Figure (2.8b) shows significant circular depressions in areas where these structures are pronounced. The karst structures are difficult to observe on time-structure map of Caddo horizon since the event is shallow but are evident on structural map of the deeper Vineyard horizon (fig 2.8a). An intersection of Inline 146 and Crossline 170 depict the evidence of these structures on vertical section, fig 2.8(b). They were postulated by Hardage et al., 1996 to be due to structural collapse of the Bend Conglomerate and each collapse is genetically related karst dissolution of the Ellenburger carbonates.

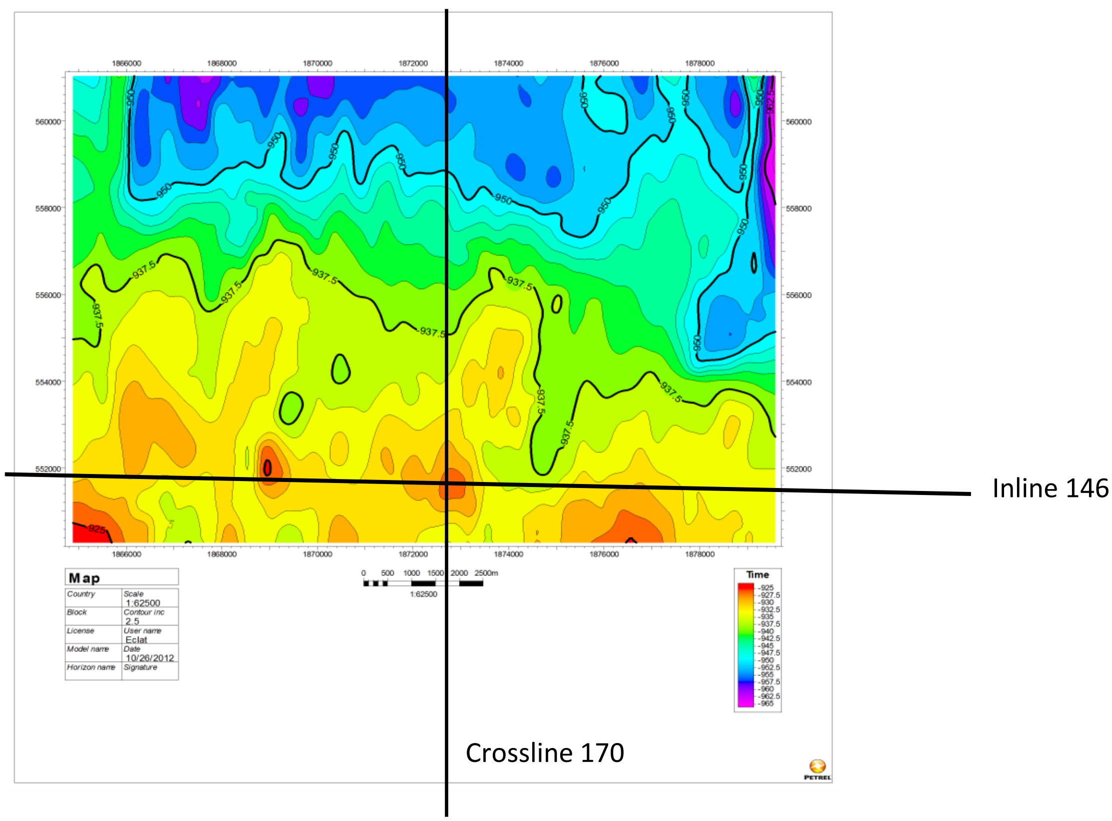

Fig 2.8(a): Time structure map (Vineyard horizon)

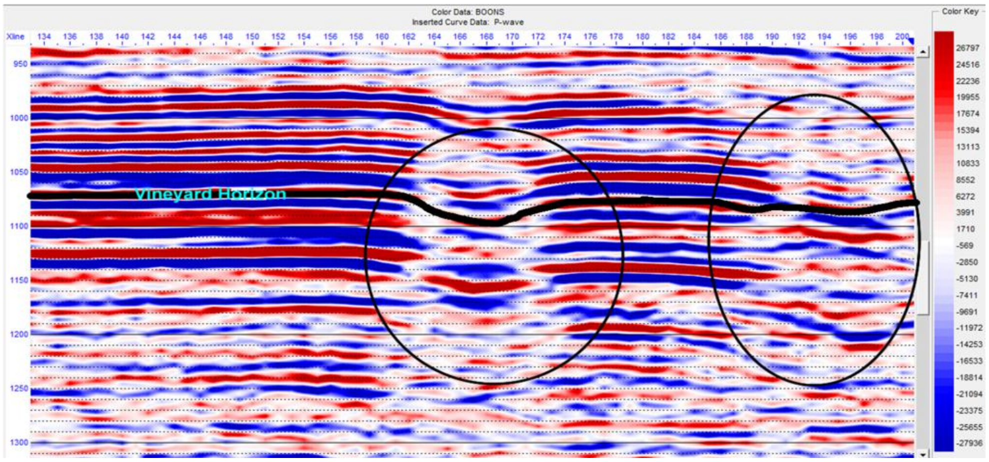

Fig 2.8(b): Inline 146 showing Carbonate dissolution (karst structures)

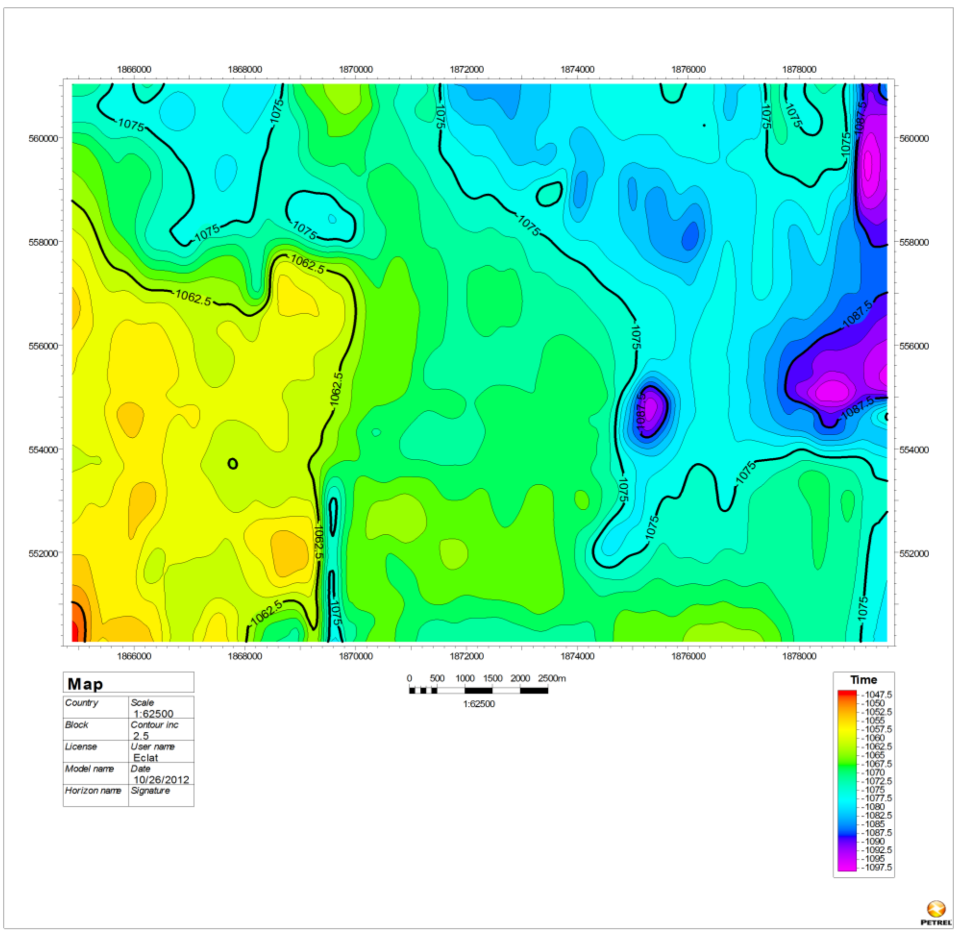

Fig 2.8(c): Time structure map (Caddo horizon)

2.3.2 RMS AMPLITUDE EXTRACTION

Even though structural information in a field is derived primarily from structural maps (time and depth) while the response to fluid in a reservoir can be delineated from amplitude information, significant loss in amplitude is observed on karst-dominated areas (indicated by the black arrows in fig 2.9).

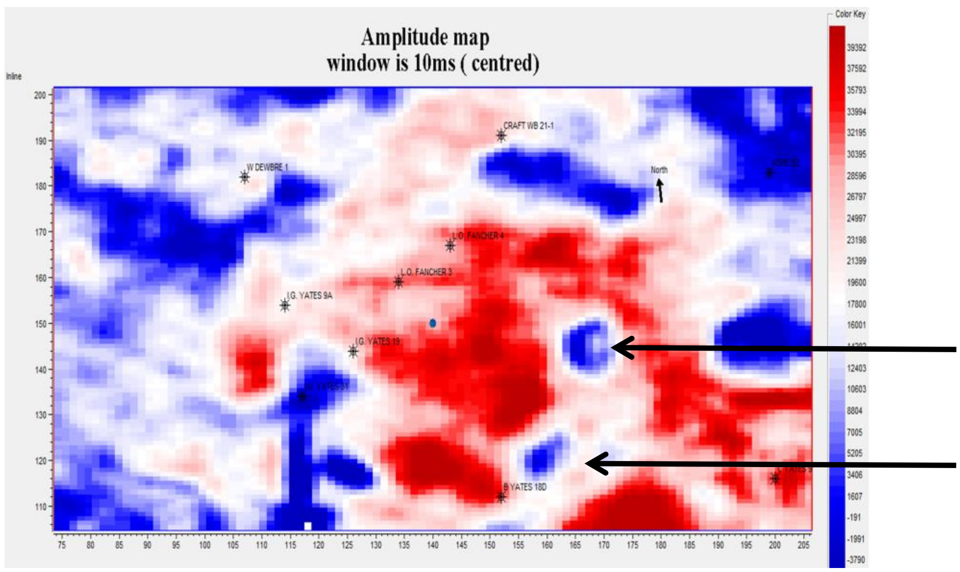

Fig 2.9: RMS amplitude off Vineyard horizon

2.4 SEISMIC MODELLING

Wedge models are applied in Exploration Geophysics in the study of seismic resolution and thin-bed analysis. The concept often aids seismic interpretation: however these models are usually oversimplified because acoustic case is often put into perspective rather than elastic. Moreover, in many modeling experiments, only primary reflections are analyzed. Wedge models used for this work are acoustic and adopt the conventional Widess method of thickness estimation. The wedge models have thickness varying from 0-30ft (0-9.1m), convolved with a Butterworth wavelet of frequencies (5-10-40-60 Hz) and also a statistical wavelet extracted from seismic. Velocity and density information are derived from Blocked logs in the vicinity of the reservoir investigated, 5660-5690ft (1725-1734m). The top of high-impedance sands in the clastic section of the field is a peak on synthetic while the base is a trough. By mapping these events on the thickness varying synthetic (offset synthetic), root-mean-square (RMS) amplitude values off the top and base of the unit are computed, and consequently plotted as function of thickness between the layers, figures (2.10a-2.10d).

The experiment is repeated for oil- and gas-charged reservoirs: results derived from tuning thickness plots are close to the Widess' theory which ranges from 52-59ft (16-18m): a quality control to the modeling experiment is the direct calculation of limit of seismic resolution (λ/4), the calculated thickness is 56ft (17m).

(A)

	Vp (m/s)	Density(g/cc)
Shale Top	3845	2.3
Gas Sand	4327	2.45
Shale Base	3845	2.3

(B)

	Vp(m/s)	Density (g/cc)
Shale Top	3845	2.3
Oil Sand	4966	2.66
Shale Base	3845	2.3

Table 2.1(a): modeling parameter for gas-charged reservoirs

Table 2.1(b): modeling parameter for oil-charged reservoirs

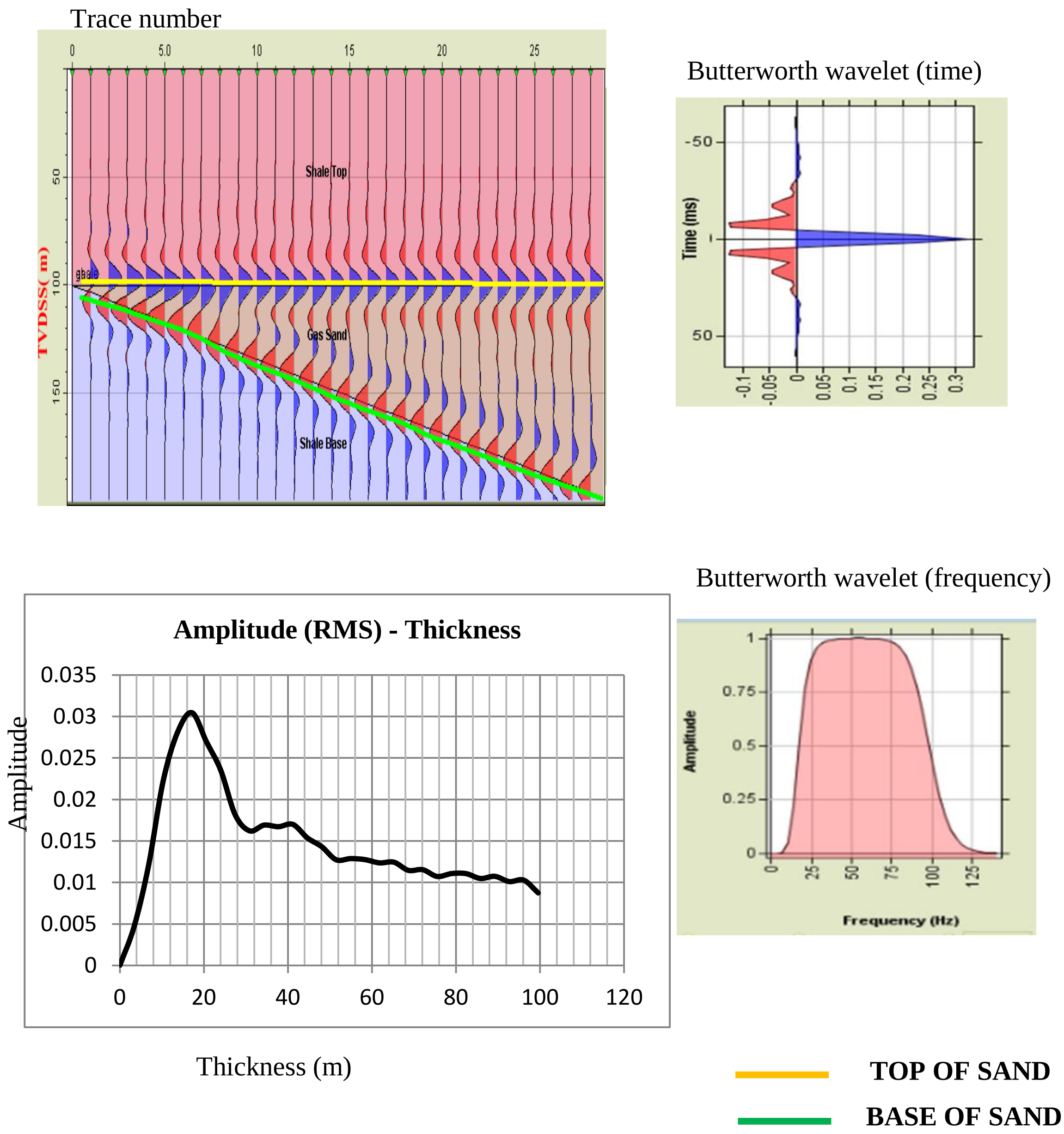

Fig 2.10(a): Wedge model created for high velocity gas sand with a Butterworth wavelet (tuning thickness = 17m)

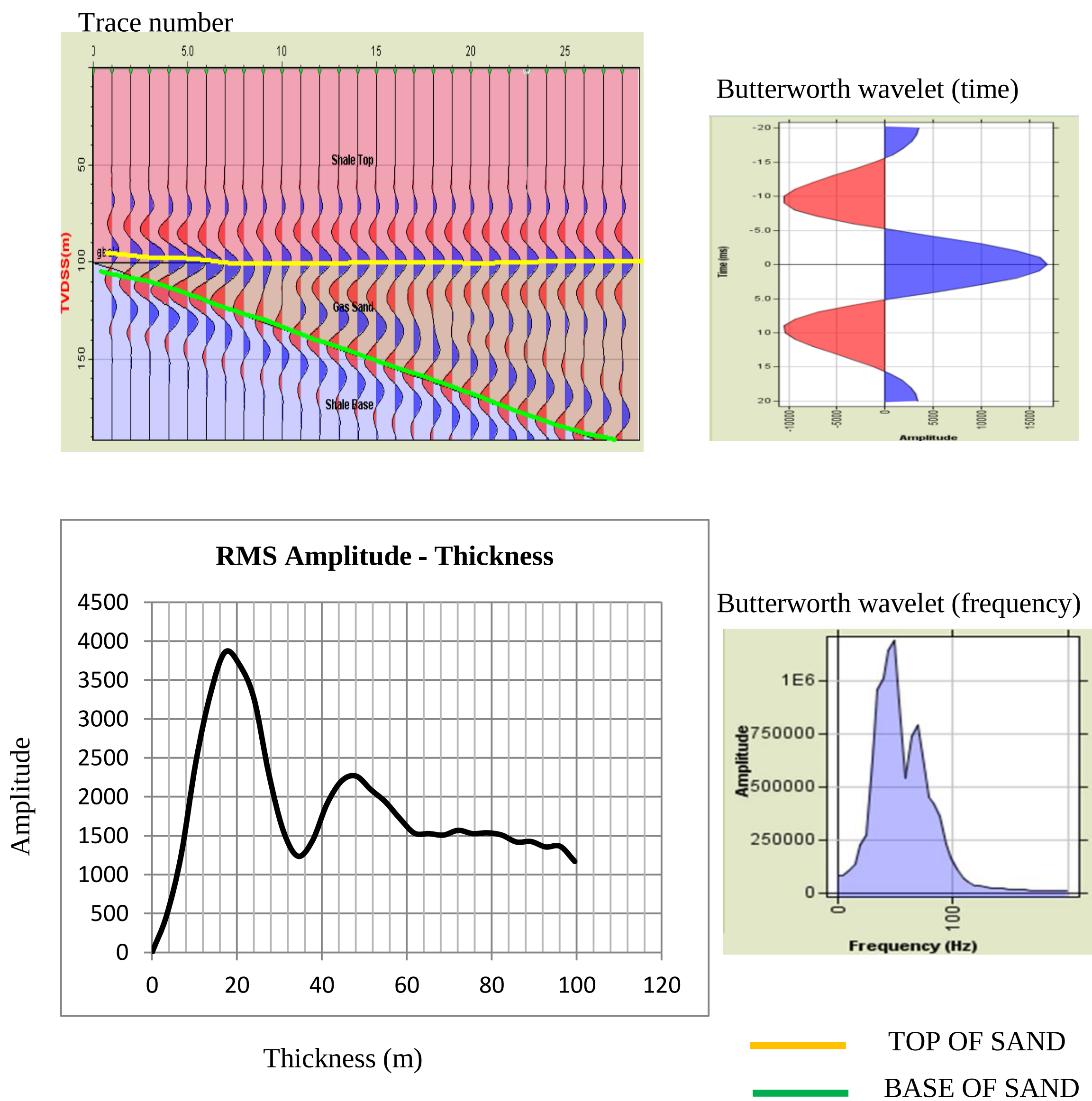

Fig 2.10(b): Wedge model created for high velocity gas sand with a wavelet extracted in the vicinity of the well (tuning thickness = 18m)

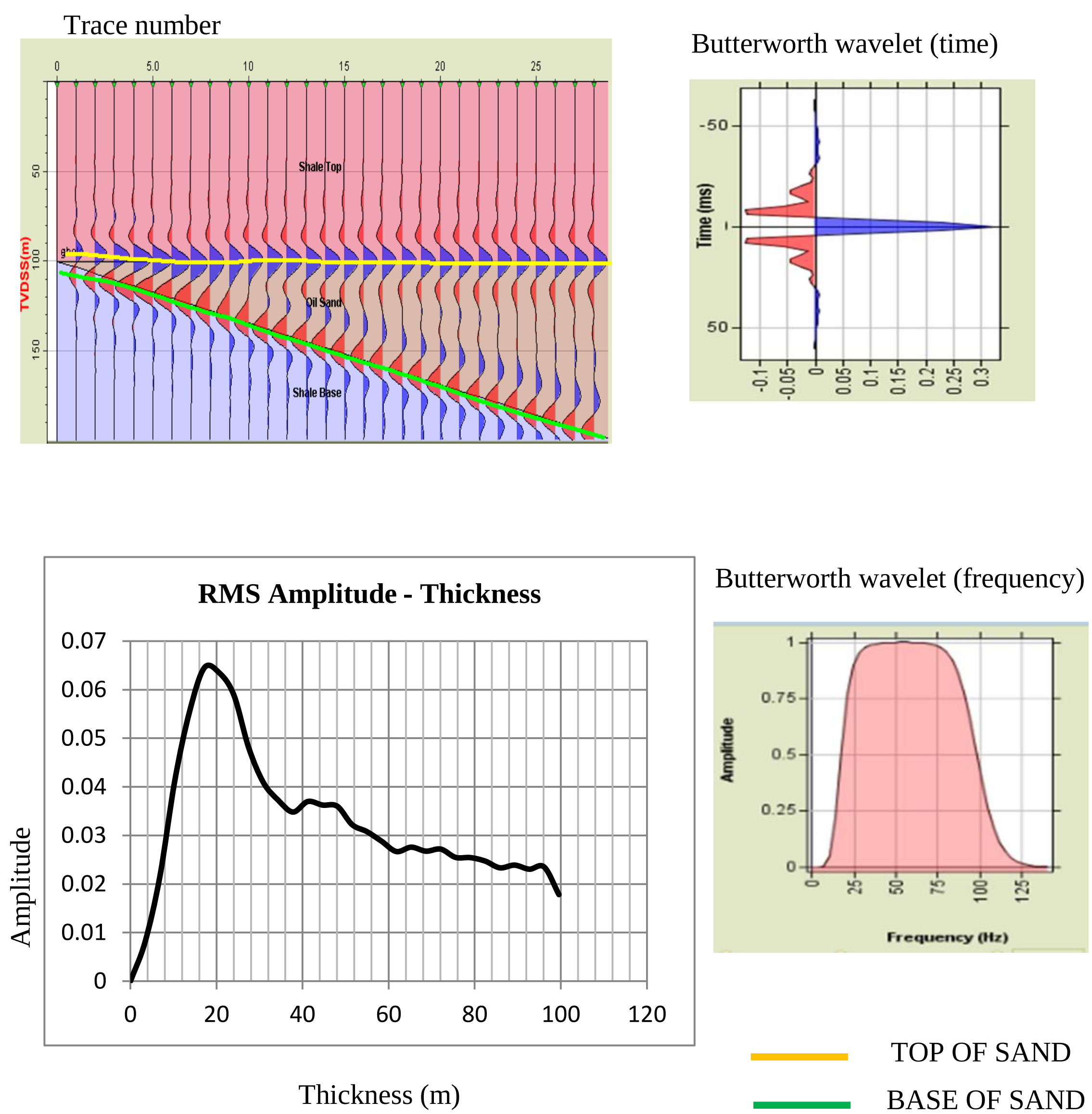

Fig 2.10(c): Wedge model for high velocity oil sand with a Butterworth wavelet (tuning thickness = 18m)

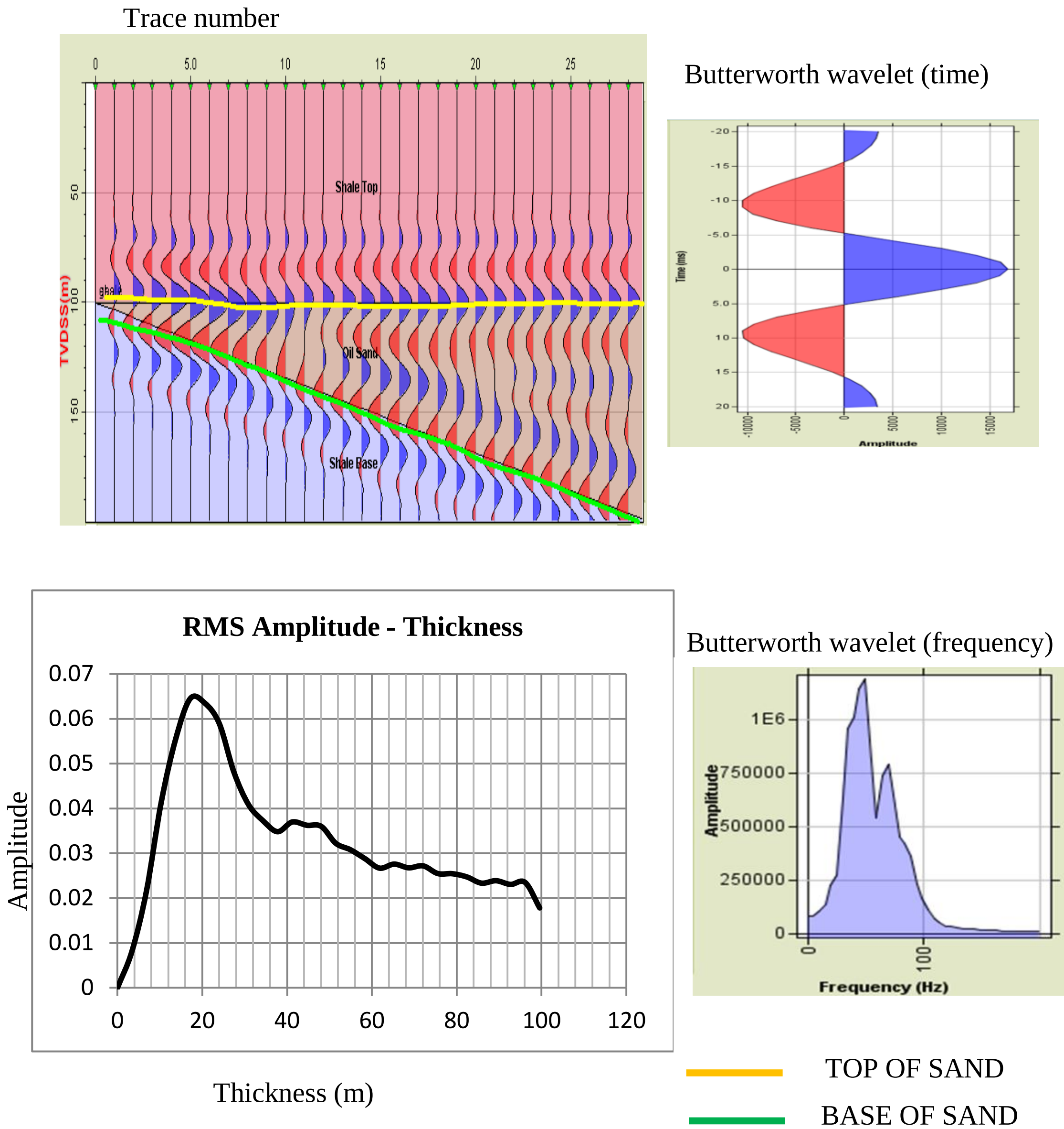

Fig 2.10(d): Wedge created for high velocity oil sand with a Butterworth wavelet (tuning thickness = 18m)

CHAPTER 3

SPECTRAL DECOMPOSITION AND INVERSION METHODS

3.0 INTRODUCTION (FOURIER TRANSFORM)

Fourier transform describes any method that results in the conversion of seismic trace in time domain to their frequency spectrum. The digital form of seismic trace is time series which can be completely described as a discrete sum of a number of sinusoids, each with unique amplitude, frequency, and phase lag (relative alignment). The analysis of a seismic trace into its sinusoidal components is achieved by forward Fourier transform (Yilmaz, O., 2001). In essence, the Fourier theory provides a means to represent arbitrary functions as a superposition(sum or integral) of a set of simpler functions called basis functions which are usually trigonometric sines and cosines of different frequencies (Gary, 2003).

The frequency domain representation of a time series often illustrates many features that are difficult to visualize in the time domain, moreover frequency domain implementation usually have greater flexibility and computational efficiency than time domain operations. Hence seismic processing algorithms are implemented with ease in this domain rather than time.

The manner in which time series is mapped into the frequency spectrum determines the amount of new information that can be obtained: standard Fourier analysis of seismic traces is a tool for processing seismic data to suppressing multiples and ground rolls through processes such as frequency filtering (Claerbout, 1976; Yilmaz, 2001), deconvolution (Lackoff and Leblac, 1975; Webster, 1978; Arya and Aggarwal, 1982). Tanner et al., 1979 uses instantaneous spectral attribute to describe changes in spectral behavior of seismogram. Partykal et al., 1999, and Sinha et al., 2005 extend this principle to detecting subtle stratigraphic features below conventional seismic resolution limit, reservoir delineation, and stratigraphic visualization (Marfurt and Kirlin, 2001**).**

Spectral decomposition is also used as a hydrocarbon indicator (Burnett et al., 2003; Castagna et al., 2003; Fahmy et al., 2005, and Sinha et al., 2005). Seismograms whose spectral content vary significantly with time are considered non-stationary and require non-standard methods of decomposition. In a stationary time series, the amplitude and phase spectra of a whole seismogram represent the frequency behavior averaged over the time. A more complete description of the time-variant frequency content requires decomposition into 2D frequency-time space. In this way, the full spectra bandwidth is described for each time sample and can be used to distinguish superimposed seismic events (Chakraborty and Okaya, 1995). Since the time-frequency decomposition of seismic data is a non-unique technique, various methods exist for time-frequency analysis of non-stationary signals. These methods of decomposition used in the course of this research are: short-time Fourier transform (STFT), continuous wavelet transform (CWT), and constrained least-squares spectral analysis (CLSSA).

3.1 SHORT-TIME FOURIER TRANSFORM (STFT)

Frequency changes with time in a non-stationary signal and the conventional Fourier transform gives the overall frequency behavior; hence the amplitude spectrum of the Fourier transform indicates the presence of different frequencies but does not show temporal resolution (Chakraborty and Okaya, 1995). STFT entails the use of a windowed function to convert a discrete time series to its equivalent frequency domain (Cohen, 1995).

Mathematically STFT can be represented by the inner product of the signal f(t) and a time-shifted windowed function and the Fourier transform of this windowed function is now computed.

$$STFT\ (\omega, \tau) = \langle F(t) \emptyset\ (t - \tau) e^{-i\omega t} \rangle \tag{3.1}$$

$$STFT\ (\omega, \tau) = \int_{-\infty}^{\infty} f(t)\ \overline{\emptyset}\ (t - \tau) e^{-i\omega t} dt \tag{3.2}$$

The time-frequency analysis is done by taking a short segment of the signal and performing Fourier transform on the windowed data to obtain local frequency information (Sinha et al., 2005). Conversely, STFT can also be implemented in the frequency domain by choosing frequency domain windows instead of sampling the time with moving windows. The frequency axis can be sampled by a set of fixed bandwith band-pass filters whose center frequency are distributed uniformly along the frequency axis (Chakraborty and Okaya, 1995).

The set back to STFT is the fixed analysis window, and the analysis window function plays an important role in the technique. If this function has a long duration in time, this implies a fine sampling of the frequency axis, and any subtle variations in the frequency content of the signal will be well resolved in the resulting 2-D STFT plot. However, because of the long time duration, small changes in the time domain become obscured because of averaging. The opposite is true for a window function of short time duration that defines short variations in time but fails to detect subtle frequency changes. This tradeoff in time-frequency resolution is known as the uncertainty principle or Heisenberg inequality, which states that the product of temporal and frequency resolution is constant: so increasing resolution in one domain consecutively decreases in the other. Hence, once a window function has been chosen for an STFT, the time-frequency resolution is fixed over the entire time-frequency spectrum analysis, thereby making the resolution of seismic data dependent on user specified window-length (Chakraborty and Okaya, 1995).

Partyka et al.(1999) provides a phase independent approach to determining the limit of seismic vertical resolution. His method developed on Widess tuning thickness model that required detailed processing for wavelet phase and accurate amplitude determination from trace to trace.

The premise behind spectral decomposition as thin-bed analytic tool is that reflections from thin layers have a unique signature in the frequency domain that is indicative of time thickness (fig 3.1). The amplitude interference spectrum delineates thin bed variability via spectral notching patterns (fig 3.4), while the phase spectrum responds to lateral discontuity via local phase instability (Partyka et al., 1999).

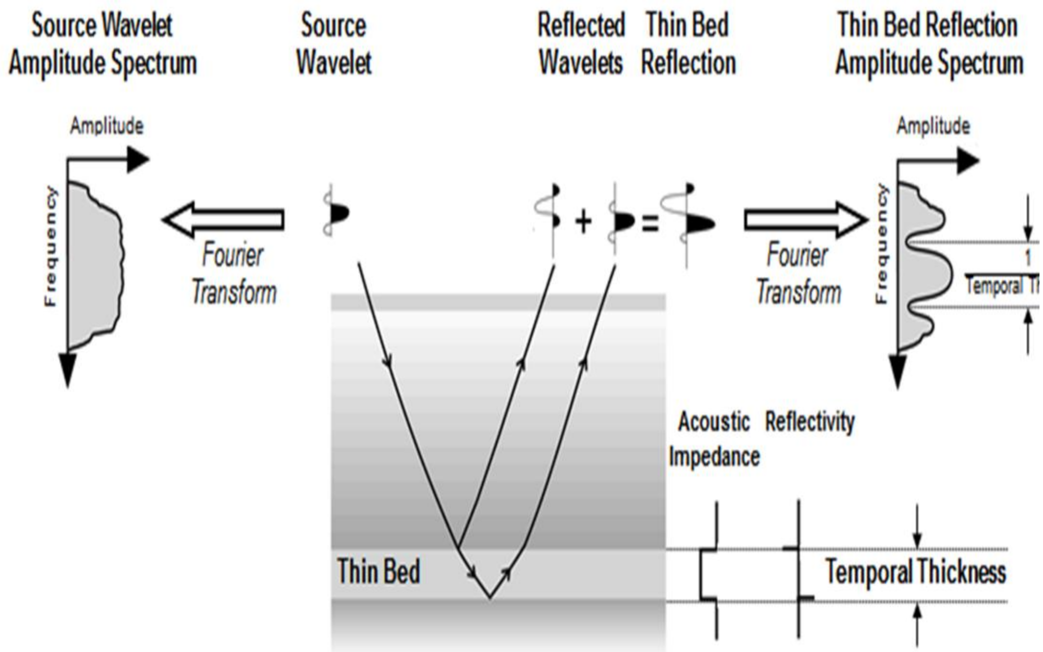

Fig 3.1: Thin bed spectral imaging (modified after Partyka et al., 1999)

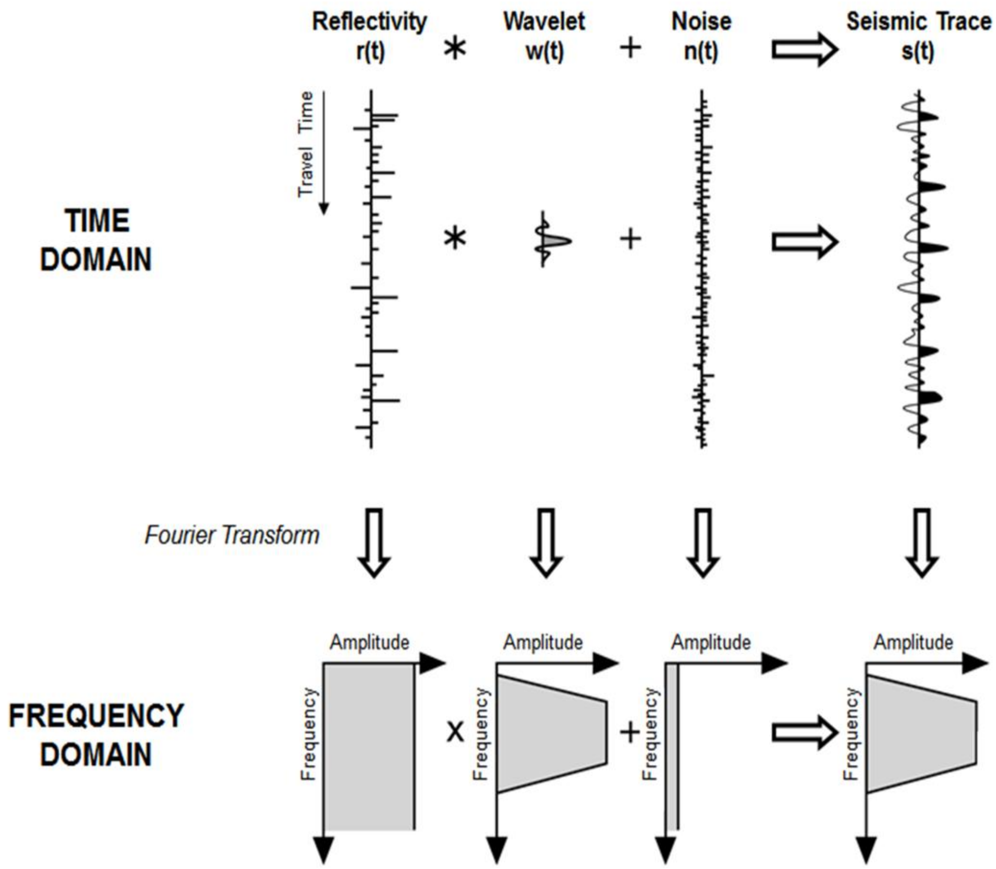

Fig 3.2: Long window spectral decomposition and its relationship with the convolutional model (modified after Partyka et al., 1999)

Since seismic data is a discrete time series, decomposition into the Fourier domain can be done by using an analysis window and consequently assigning the spectrum derived from that window to the center of the time analysis. Windowing length can be either long or short depending on the type of information one is interested in. Long enough windows approximates the earth to be random since it comprises of stacked geologic thin layers (fig 3.2). The consequence of the randomness assumption of the stacked geologic layers is the generation of white spectrum.

Hence, convolution of a wavelet using a long window length (stacked geologic layers) creates amplitude spectrum that resemble the source wavelet (fig 3.2).

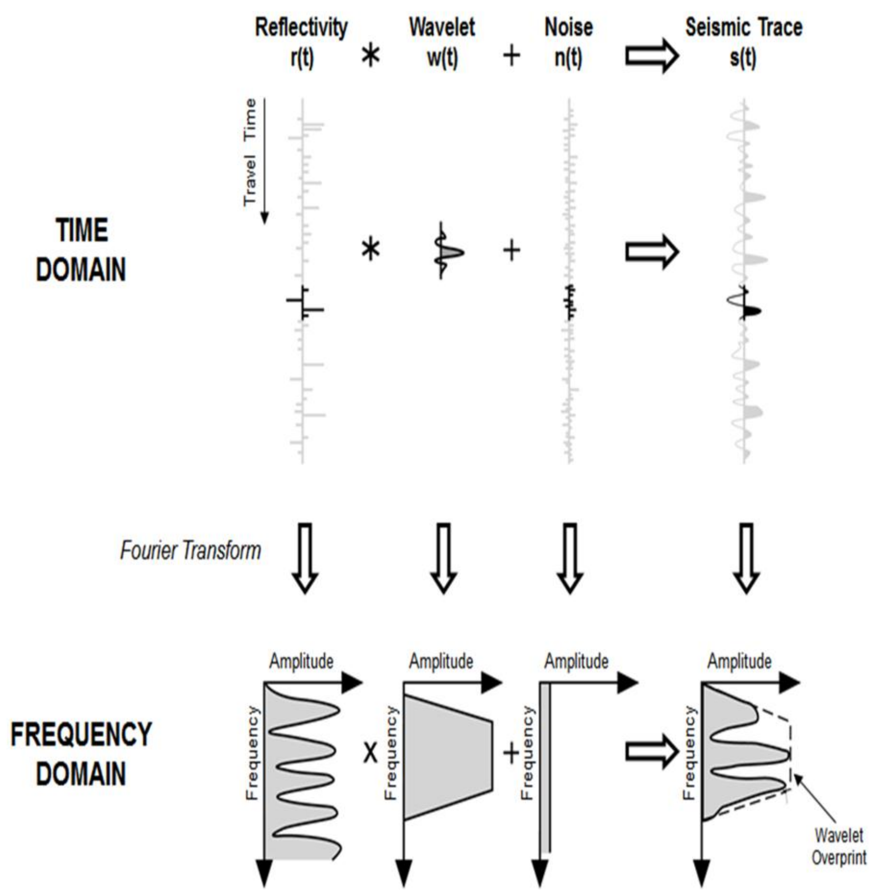

Fig 3.3: Short window spectral decomposition and its relationship with the convolutional model (modified after Partyka et al., 1999)

Partyka showed that applying a short window length provides better geologic detail. The STFT gives a spectrum that is not white but dependent on the acoustic properties and thickness spanned by the window (fig 3.3). The smaller the window length, the less random and better the geologic information derived from spectral analysis. This method provides insights in delineating subtle stratigraphic information such as channels etc. that would otherwise be obscured in conventional seismic section.

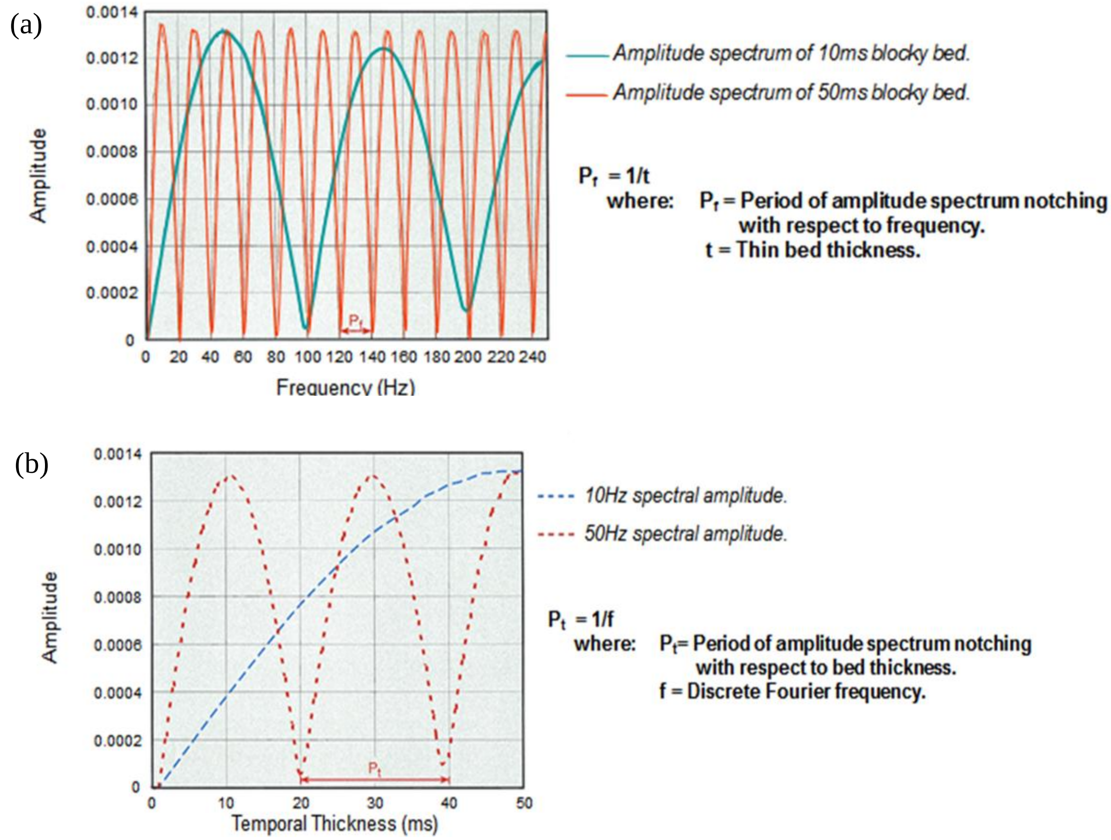

Fig 3.4: Thin-bed tuning of amplitudes versus frequency

(a) with respect to frequency

(b) with respect to thin-bed thickness

(modified after Partyka et al., 1999)

3.2 CONTINUOUS WAVELET TRANSFORM (CWT)

Continuous wavelet transforms attempts to solve the fundamental problem of short-time Fourier transform by examining the frequency distribution of non-stationary time series with a set of windows that have compact support in time and are band-limited. These window functions are wavelets because they resemble tiny waves that grow and decay in short period of time (Chakraborty and Okaya, 1995). A wavelet can also be defined as finite energy function with a zero mean, localized in both time and frequency. Continuous wavelet transform is the projection of a wavelet on a continuous family of frequency bands. In CWT, wavelets scale in such a way that the time support changes for different frequencies: smaller time (compressions) support increases the frequency support while larger time supports (dilation) support decreases the frequency support. By dilating and translating the wavelet, a family of wavelet $\psi_{\sigma,\tau}(t)$ is produced, given by:

$$\psi_{\sigma,\tau} = \frac{1}{\sqrt{\sigma}}\Psi(\frac{t-\sigma}{\sigma}) \tag{3.3}$$

Where σ, τ are real numbers and σ is not zero, σ and, τ are called the scale and translation parameters respectively. The wavelet is normalized such that $\|\psi\|$is equal to unity. CWT is defined as the inner product of a family of wavelets $\psi_{\sigma,\tau}(t)$ with the signal f(t), shown mathematically by:

$$F_w(\sigma,\tau) = \langle f(t), \psi_{\sigma,\tau\,(t)}\rangle = \int_{-\infty}^{\infty} f(t)\frac{1}{\sqrt{\sigma}}\bar{\psi}\left(\frac{t-\tau}{\sigma}\right)dt \tag{3.4}$$

Where $\bar{\psi}$ is the complex conjugate and F_w is the time-scale map. In reconstructing the original signal f(t) from the wavelet transform, Calderon's identity is used (Torrence and Compo, 1998)

$$\psi_o\ (t) = \ \pi^{-1/4}\ e^{iw_o t}\ e^{-t^2/2} \tag{3.5}$$

A kernel wavelet is required to satisfy the admissibility criteria for the inverse transform to take place, this is given by:

$$c_\psi = 2\pi\int_{-\infty}^{\infty}\frac{\|\hat{\psi}(\omega)\|^2}{\omega}d\omega < \ \infty \tag{3.6}$$

Morlet wavelet satisfies these conditions and is commonly used in continuous wavelet transform. The result of the transformation is a time-frequency scale, a scalogram. Interpreting a scalogram is not intuitive and thus requires a means of transforming the frequency band (scale) to discrete frequencies that are interpretable. One of the methods of interpreting time-scale map is stretching of the scale to an equivalent frequency depending on the scale-frequency mapping of the wavelet (Hlawatsch and Bartels, 1992).

Sinha et al. (2005) adopted the unique resolution property (adaptive window) of a Morlet as a means of reconstructing the frequencies. Morlet wavelet's adaptive translational property gives good frequency resolution at low frequencies and high time resolution at high frequencies. This property enables the ability to observe the frequency content at various times, thus leading to time-frequency map that is adaptive to the non-stationary nature of seismic signals. This can be computed by taking the Fourier transform of the inverse continuous wavelet function (Sinha et al., 2005). The basic equation for computing time-frequency continuous wavelet transform (TFCWT) is shown below:

$$\hat{f}(\omega,\tau) = \frac{1}{C_\psi}\int_{-\infty}^{\infty} F_\omega(\sigma,\tau)\hat{\psi}\, e^{-i\omega\tau}\,\frac{d\sigma}{\sigma^{3/2}} \qquad (3.7)$$

The computational process is in two-fold:

- Computation of the convolutional integral to obtain $F_w(\sigma,\tau)$ using the Fourier method.
- Fourier transformation of the scaled and modulated wavelet to compute inner product over all scales.

In conventional continuous wavelet transform, time-frequency is computed from scalogram in terms of frequency bands (scales) by taking the center frequency of the bands. The disadvantage of this method is that the frequencies overlap and there is apparent loss of energy in the spectrum that can be misinterpreted as attenuation effects. The time-frequency map yield energy at the desired frequency and avoids complications due to overlapping frequency bands unique to scale-frequency transformation. Thus TFCWT has high frequency resolution at low frequency and high time resolution at high frequency that makes it very ideal for several applications especially in detecting low frequencies beneath gas sand (Sinha et al., 2005).

3.3 CONSTRANIED LEAST-SQUARES SPECTRAL ANALYSIS (CLSSA)

Fourier series decomposes a periodic function into infinite number of sines and cosines with different frequencies and amplitude. The coefficient of the series is determined by analyzing the orthogonality property of the sinusoids. Development of Fourier series is the motivation for the Fourier transform. Fourier transform is one of the ways for solving the coefficients of the Fourier series by applying the least-squares solution. The main assumption is that the basis sinusoidal functions are uncorrelated (Puryear et al., 2012).

Time-frequency decomposition implemented with either CWT, STFT suffers from a trade-off between temporal and frequency resolution. As discussed earlier, STFT applied a windowed-function to discrete time series for conversion into the frequency domain (Chakraborty and Okaya, 1995; Cohen, 1995).Windowing a seismic trace is expedient in time-frequency analysis to account for the time-variant nature of seismic data. This trade-off in resolution is known as Heisenberg uncertainty principle.

Puryear et al.(2012) approach to solving the windowing problem inherent in decomposing non-stationary signals entails bypassing the Fourier transform and solving for the coefficients of the Fourier series directly. The least-squares solution of the Fourier series (Fourier transform) does not hold for some frequencies when the window length is not an integer of periods, the upshot is energy smearing across the window. Noteworthy is the fact that Fourier transform (a process of solving for Fourier series coefficients with least-squares method) is not responsible for energy smearing; rather it is the implicit requirement that the basis function must be uncorrelated. Energy smearing seen when Fourier transform is applied to windowed segment of the data yield the spectrum of the window rather than the spectrum of the data within the window (Puryear et al., 2012).

CLSSA attempts to solve Fourier series coefficients within a window by applying apriori constraints on the inversion process that will compensate for the non-orthogonality of the basis function within that window.

Starting with a forward model, $Fm = d$ (3.8)

$$d = dr + id_i \quad (3.9)$$

F is the kernel matrix, m is the model parameter and d is the windowed seismic data which can also be represented as a complex seismic trace to effect optimum stabilization of the result for small window length. The solution to equation above is F*Fm = F*d, where F is complex sinusoidal signal truncated by the endpoints of the windows in the time domain and F* is the complex conjugate.

The least mean square error (LMSE) solution to equation (3.8) is

$$m = (F^*F)^{-1} F^*d \quad (3.10)$$

If the sinusoids are uncorrelated, then F*F=I (identity matrix) and equation (3.10) becomes

m = F*d, this is the Discrete Fourier Transform (DFT) equivalent of the signal if the aforementioned conditions are met. But windowing the dataset makes the elements of the kernel to be uncorrelated and hence require constraints to achieve a unique solution.

A priori constraint into the inversion involves the introduction of two kernel matrices W_m and W_d (model and data weights).The model weights (W_d) changes iteratively while the data matrix (W_m) remains constant. Applying model and data weights to the basic equations (3.8) gives:

$$W_dW_mF = W_dW_md \quad (3.11)$$

$$W_dFW_m(W_m)^{-1} = W_dd \quad (3.12)$$

Substituting weighted quantities ($F_W = W_dFW_m$ and $m_w = W^{-1}{}_m$) and showing equation (3.13) as weighted ill-posed inverse problem give equation (3.13).

$$F_mW_m = W_dd. \quad (3.13)$$

Equation (3.13) must be initially reformatted as a well-posed minimization problem that can be solved by defining Tikhonov parametric functional in the space of the weighted model parameter (Portniaguine and Zhdanov, 1999):

$$\| F_w m_w - W_d d\|^2 + \alpha \|m_w\|^2 = \min \qquad (3.14)$$

Where α is a regularization parameter that can be varied to control the sparsity and stability of the solution. The Lagrange solution to equation (3.14), (Portniaguine and Zhdanov, 1999) and matrix inversion of the solution computed by Gaussian elimination is shown below.

$$m_w = F_w^*(F_w F_w^* + \alpha I)^{-1} W_d d \qquad (3.15)$$

$$m = W_m m_w \qquad (3.16)$$

m is the computed frequency spectrum of the data. This is the basic approach to constrained least-squares spectral analysis (CLSSA). For more detailed study of the technique with vast amount of case histories demonstrating the efficacy of this novel method of spectral decomposition, the interested reader is referred to Puryear et al.(2012).

3.4 SPECTRAL INVERSION THEORY

Creating better seismic images by enhancing the reflection detail while improving resolution is a sought after property for seismic analysis. The seismic wavelength which is approximately 78m (depending on frequency content of the data) is often unable to resolve subtle stratigraphic features that are less than 40ft (12m) in the reservoir or even illuminate the reservoirs itself in time. This has imposed a level of uncertainty in estimating important parameters (net-gross, lithology) in reservoir models. Earlier research by Widess utilizes amplitude to calibrate reservoir thickness but the method fails below the tuning thickness as described by Widess to be λ/4. In the frequency domain, Partyka (2001) summarizes three methods of phase-independent thickness estimation using spectrally-decomposed data. These methods spans from spectral decomposition derived dominant frequency, dominant amplitude mapping, and spectral decomposition derived thickness via discrete Fourier components.

Puryear and Castagna (2008) employed the notch pattern observed in the amplitude spectrum of a thin-bed as an inversion problem for reflectivity; the underlying principle is the determination of layer thickness using the periodicity of notches in the amplitude spectrum. The inversion for layer thickness utilizes the theory of complex trace analysis to delineate accurate thickness estimation below tuning by applying the inverse relationship between thickness and constant periodicity of spectral interference patterns.

3.4.1 SEISMIC RESOLUTION (ODD AND EVEN REFLECTION COEFFICIENT)

Conventional intuition from Widess (1971) portrayed a restricted workflow for thin-bed analysis. The basic conclusions from Widess's models presuppose that seismic character (peak/trough time) and frequency does not change with thickness and amplitude varies almost linearly with thickness which slowly decline to zero at zero thickness.

Tirado (2004) offered another insight into traditional view of reflection reflections pairs by showing that a reflection coefficient can be decomposed into odd and even components, with the even components having equal magnitude and sign while the odd components have equal magnitude but opposite sign (fig 3.5). The odd components interfere destructively thereby limiting resolution while the even components interfere constructively enhancing seismic resolvability.

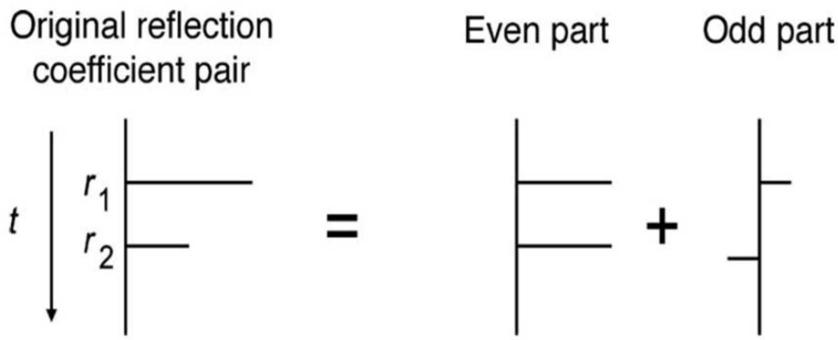

Fig 3.5: Representation of any arbitrary reflection coefficients (r_1 and r_2) by the summation of odd and even components (modified after Puryear and Castagna, 2008)

Widess model was based primarily on the odd component; thereby ascribing the conventional resolution limit to λ/4. Although this assumption is true for sand encased in shale, the presence of a small amount of the even component contributes immensely to resolution.

In contrary to Widess's conclusion on the variation of amplitude and frequency with thickness: analysis of peak frequency and amplitude from equations derived by Chung and Lawton (1995) showed that the amplitude extend well beyond the theoretical limit (fig 3.6). This new insight, coupled with novel phase-independent thickness estimation method from amplitude spectrum work by Partyka et al.(1999), form the motivation for a more robust workflow for delineating reservoir thickness beyond the conventional limit of seismic resolution.

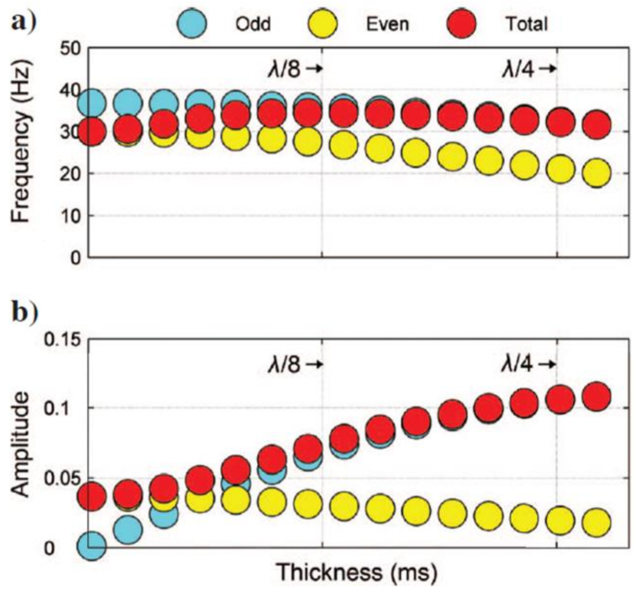

Fig 3.6: Resolution test using odd and even component of reflection coefficients

(a) Peak frequency as a function of thickness

(b) Peak amplitude as a function of thickness

(Modified after Puryear and Castagna, 2008)

3.4.2 DEFINITION OF SPECTRAL INVERSION PARAMETERS

Spectral inversion theory utilizes complex trace analysis to develop an algorithm that invert for bed thickness from periodicity of the notches in the amplitude spectrum (Puryear and Castagna, 2008). Marfurt and Kirlin (2001) define time domain impulse function or Green's function g(t) as :

$$g(t) = r_1\,\delta(t - t_1) + r_2\delta(t - t_1 - T) \tag{3.17}$$

Where r_1 is the angle dependent reflection coefficient from the top of a thin bed, r_2 is the reflection coefficient off the bottom of a thin bed, t is time sample, t_1 is time sample at the top reflector and T is the layer thickness. Analyzing the Green's function at the center of the layer, applying Fourier transform, and consequent simplification using trigonometric identities.

Equation (3.17) is divided into its real(Re) and imaginary part(Im):

$$Re[g(f)] = (2r_e)\cos(\pi fT) \qquad (3.18a)$$

$$Im[g(f)] = (2r_o)\sin(\pi fT) \qquad (3.18b)$$

Where r_e is the even component and r_o is the odd component.

Placing the point of analysis symmetrically at the center of layer ensures the constant period in the spectrum which divides the reflection coefficient into perfectly odd and even components that eliminates phase variation. In order to shift the point of analysis away from the center of the layer while at the same time maintaining periodicity in the spectrum, the moduli of real and imaginary functions are computed which is insensitive to phase. The cost function is derived at each frequency by applying the shift theorem on the moduli of the real and imaginary components. The theorem states that a time sample shift (Δt) away from the center layer t_c in the time domain is equivalent to a phase ramp in the frequency domain.

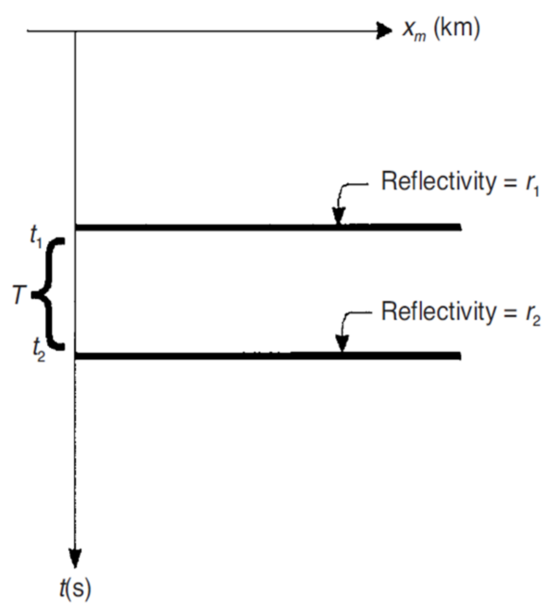

Fig 3.7: Two-layer reflectivity model (modified after Marfurt and Kirlin, 2001)

The derivation of the inversion model from amplitude spectrum in a single layer case is given by:

$$G(f)\frac{dG(f)}{df} = -2\pi TKsin(2\pi fT) \quad (3.19)$$

The solution to this equation is derived by evaluating the cost function, equation (3.20) below and searching for physically reasonable model parameters K and T or by another nonlinear iterative inversion (Puryear and Castagna, 2008)

$$O\ (t, K) = G(f)\ \frac{dG(f)}{df} + 2\pi \mathrm{TKsin}\ (2\pi \mathrm{fT}) \quad (3.20)$$

G(f) is the magnitude of amplitude as a function of frequency, $\frac{dG(f)}{df}$ is the derivative of the magnitude of the amplitude at each frequency and k = $re_2 - ro_2$.

Optimum parameters for the inversion is derived by minimizing the error between the model and the product of the magnitude of the amplitude and the derivative of the magnitude of the amplitude at each frequency. This parameter is dependent on the signal to noise ratio over the analysis band, other model parameters for equation (3.19) are given below:

$$r_o = \sqrt{\frac{G(f)^2}{4}} - kcos^2(\pi \mathrm{fT}) \quad (3.21a)$$

$$r_e = \sqrt{K + r_o^2} \ \text{ and} \quad (3.21b)$$

$$t_1 = \frac{1}{2i\pi \mathrm{f}} \mathrm{In}\left[\frac{g(f)}{r_1 + r_2 e^{2\pi \mathrm{ifT}}}\right] \quad (3.21c)$$

where t_1 is derived by taking the Fourier transform of equation (3.17) and solving for t.

The reflectivity layer model can be reconstructed from the initial parameters: K and T. By utilizing equations (3.18a and 3.18b) to reconstruct the odd and even reflections, reflections at the top (r_1) and base (r_2) can be recomputed from these components. This is the solution for a single-layer case. Puryear and Castagna, 2008 extends this principle to account for multiplicity of subsurface layers and will be discussed in the following section.

3.4.3 SPECTRAL INVERSION FOR MULTIPLE LAYERS

Extension of the inversion algorithm to multiple layers can be formulated by considering a seismogram to be made up of superposition of impulse pairs. The inversion for the properties of a single layer is extended easily to encompass a general reflectivity-series inversion by considering the spectrum versus time acquired using a moving window as a superposition of interference patterns originating at different times. The inversion for reflection coefficient and layer thickness is performed simultaneously for all impulse pairs affecting the local seismic response (Puryear and Castagna, 2008).

The reflectivity series can be represented as a sum of odd and even impulse pairs.

$$r(t) = \int_{-\infty}^{\infty} \left[r_e(t) II\left(\frac{t-\tau}{T(t)}\right)\right] dt + \int_{-\infty}^{\infty} \left[r_o I_1\left(\frac{t-\tau}{T(t)}\right)\right] dt \tag{3.22}$$

T(t) is the times series of layer thicknesses, $r_e(t)$ and $r_o(t)$ are magnitudes of impulse pairs ,I is the odd impulse pair and II is the even. The spectral decomposition of a seismic trace S(t,f) with a known wavelet w(t,f) is

$$S(t,f) = \int_{-t_w}^{t_w} \{r_e cos[\pi f T(t)] + i r_o sin[\pi f T(t)]\} dt \tag{3.23}$$

where t_w is window half-length.

The multilayer case involves more than two reflectors, so it is necessary to use an objective function for inversion that properly accounts for interference between multiple layers. The solution for reflection coefficient r(t) exist if the wavelet spectrum is known by optimizing the objective function.

$$o(t, r_e, r_{o,} T) = \int_{f_L}^{f_H} \left[\alpha_e \left\{R_e\left[\frac{S(t,f)}{w(t,f)}\right] - \int_{-t_w}^{t_w} r_e cos[\pi f T(t) dt]\right\} + \alpha_o \left\{Im\left[\frac{s(t,f)}{w(t,f)}\right] - \int_{-t_w}^{t_w} r_o sin[\pi f T(t)] dt\right\} df\right] \tag{3.23}$$

where F_L is low-frequency cutoff, f_H is high-frequency cutoff, and α_e and α_o are weighting functions, the ratio of which can be adjusted to find an acceptable trade-off between noise and resolution (Puryear and Castagna, 2008).

CHAPTER 4

CASE – STUDY RESULTS

4.0 INTRODUCTION

The aim of this research is to characterize sub-seimic reservoirs in the Boonsville field using spectral decomposition and inversion methods. This case study result can be broadly discussed under the three categories listed below:

- Comparison of thickness estimation method from spectral attribute volume and true thickness from well data (log-constrained).
- Comparison of spectral decomposition techniques (CWT, DFT, and CLSSA).
- Analysis of high resolution spectral inversion product (executed without apriori model).

4.1 COMPARISON OF THICKNESS ESTIMATION METHOD FROM SPECTRAL ATTRIBUTE VOLUME AND TRUE THICKNESS FROM WELL DATA.

The first stage of the interpretation entails overlaying a tied well log (lithologic indicator such as gamma ray) on the discrete frequency volumes and scrolling through to inspect the frequency at which the events are well resolved (thin sand formations below tuning thickness should resonate with a bright amplitude at tuning frequencies). At frequency of 25Hz (Fig 4.1), I could interpret four coherent events which I mapped to compute time structure maps.

Stratigraphic well-tops and time-depth pairs derived from seismic-well ties are used to create velocity model that converts the horizons in time to depth domain. Analyses of these results showed that thickness map generated from Horizon three and Horizon one are closer to those measured at the well location (fig 4.2).

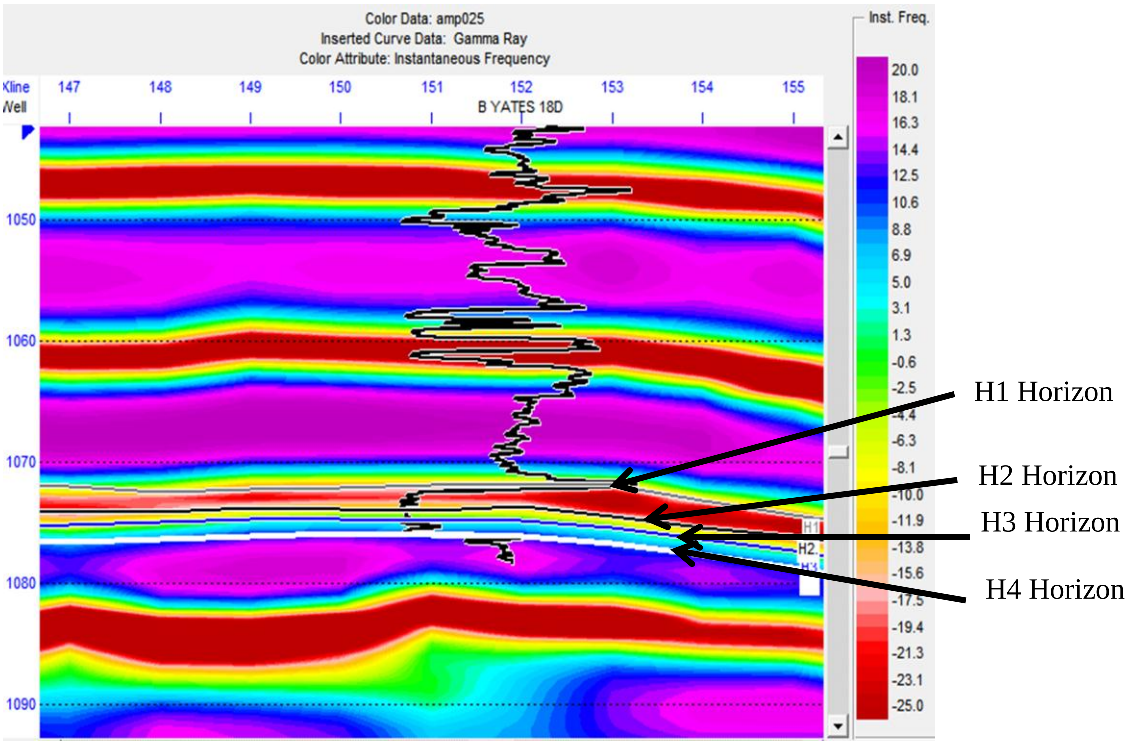

Fig 4.1: Seismic volume (25Hz) with interpreted horizons

Table 4.1 shows information on the true thickness (from logs) and calculated thickness (from spectral decomposition attribute volume), the results are well correlated. The maximum difference in thickness is observed in well BY13 which 2000m away from the survey. This method of thickness estimation produces reliable results but is highly constrained by well-logs.

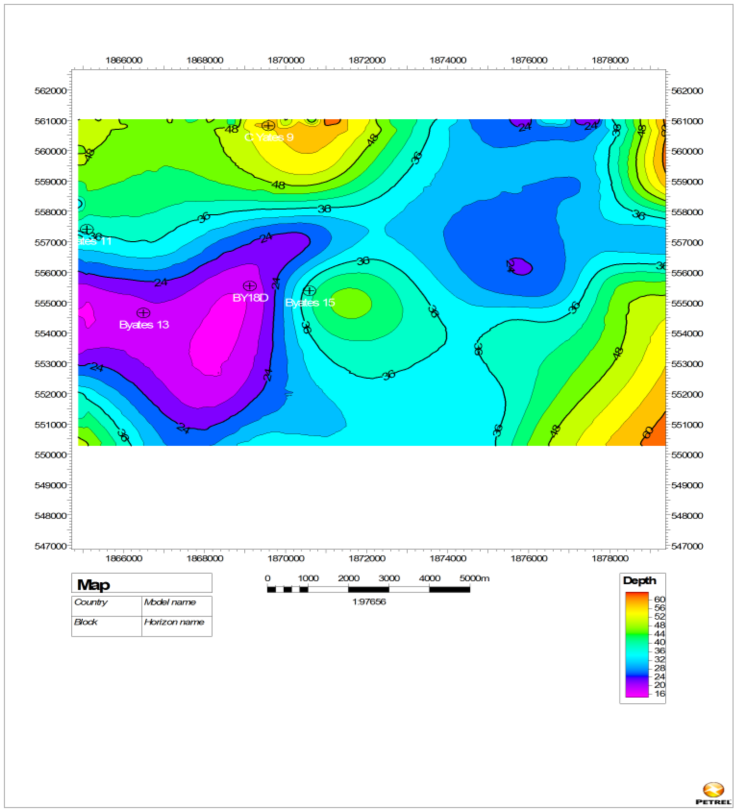

Fig 4.2: Thickness map from horizon one and three

Well Name	Well location		Original Thickness (log) ft(t)	Measured Thickness (Map) ft(t)	Differences (ft)	Offset (ft)
	Inline	Crossline				
BY 18D	112	152	27	22	5	0
BY11	75	168	37	36	1	3300
BY15	125	150	34	36	2	0
CY9	116	200	40	44	4	0
BY 13	88	143	15	22	7	2000

Table 4.1: Thickness comparison of apparent thickness (seismic attribute volume and true thickness (well-log).

4.2 FREQUENCY GATHERS

Composite traces from wells BY18D and CY9 are used to generate frequency gathers: this is a display of frequency spectrum computed from individual time samples in the traces. The gathers show energy distribution over different frequencies for a trace in time (Jochen et al., 2004). At window length of 20ms and 40ms, these gathers are computed using constrained least-squares spectral analysis (CLSSA), continuous wavelet transforms (CWT) and discrete Fourier transform (DFT). Gathers from each spectral decomposition methods are compared side-by-side to inspect for time-frequency resolution superiority. Figures 4.3 (a-b) shows two isolated events on composite traces extracted from well CY9 while fig 4.3 (c-d) shows three separate events on the traces extracted from well BY18D: the remaining panels on these figures are plots of the frequency spectrum computed from the three spectral decomposition methods.

From these figures, CWT has the least resolution of the events: this is typical of CWT showing poor temporal resolution at low frequency but better time resolution at higher frequencies. Irrespective of the window length used in decomposing the signals, CLSSA shows a more compact spectrum and also resolve the individual events on the traces. This resolution advantage makes it a better choice for decomposing the seismic data in readiness for the inversion process.

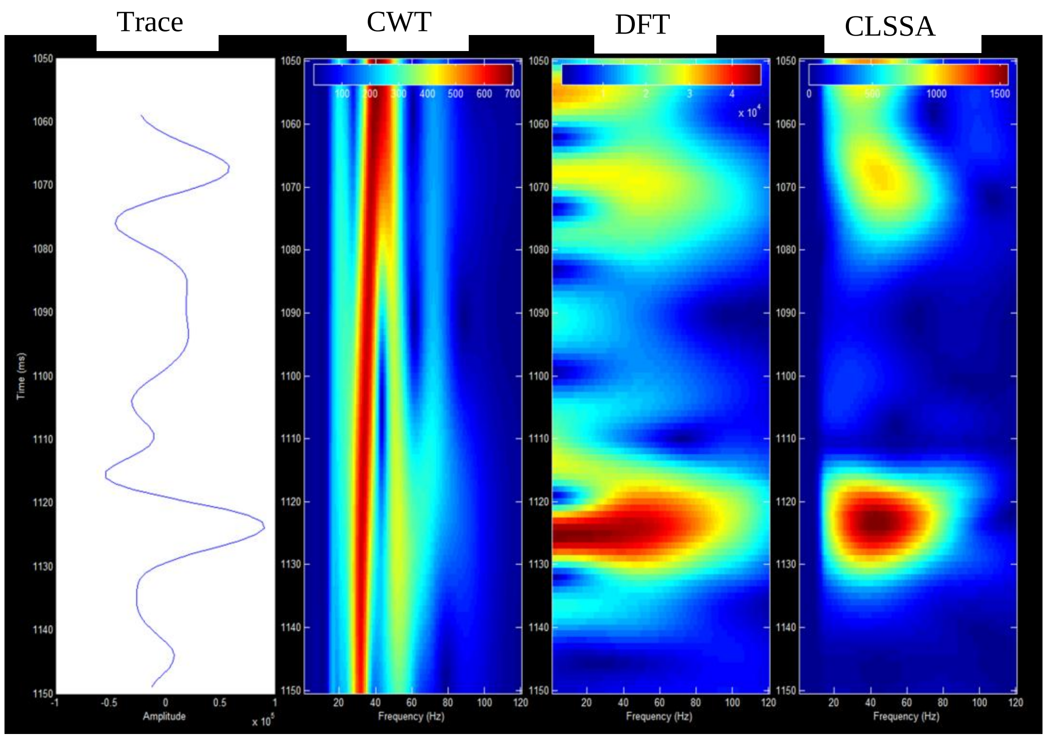

Fig 4.3a: Comparison of frequency gathers for CWT, DFT, and CLSSA with CY9 composite trace using 20ms window

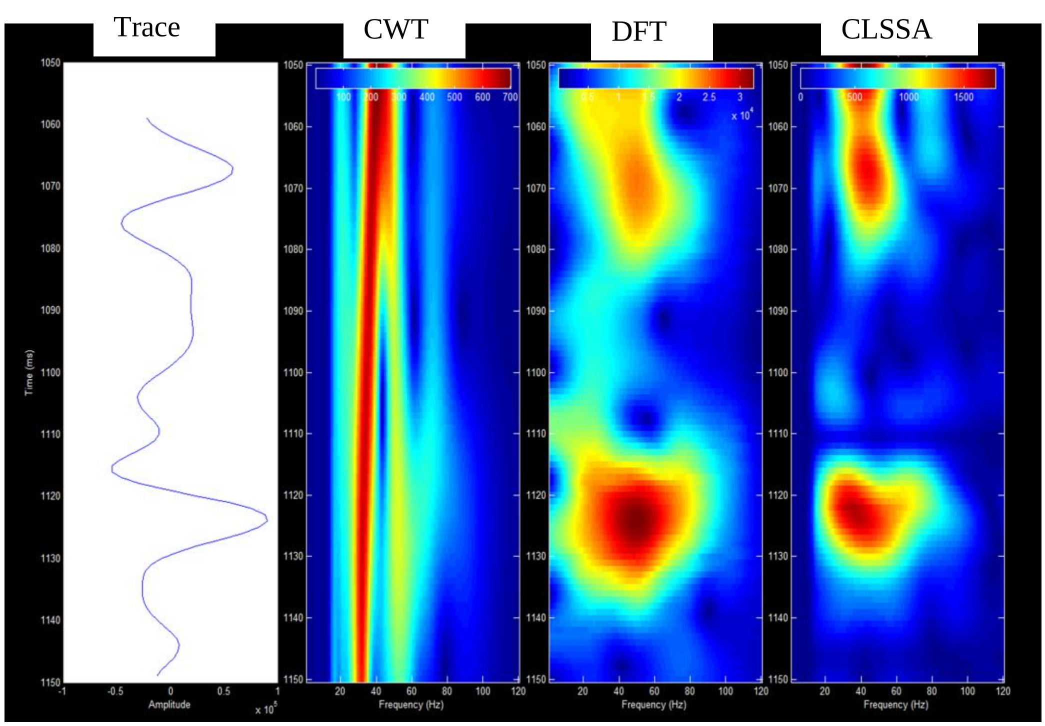

Fig 4.3b: Comparison of frequency gathers for CWT, DFT, and CLSSA with CY9 composite trace using 40ms window

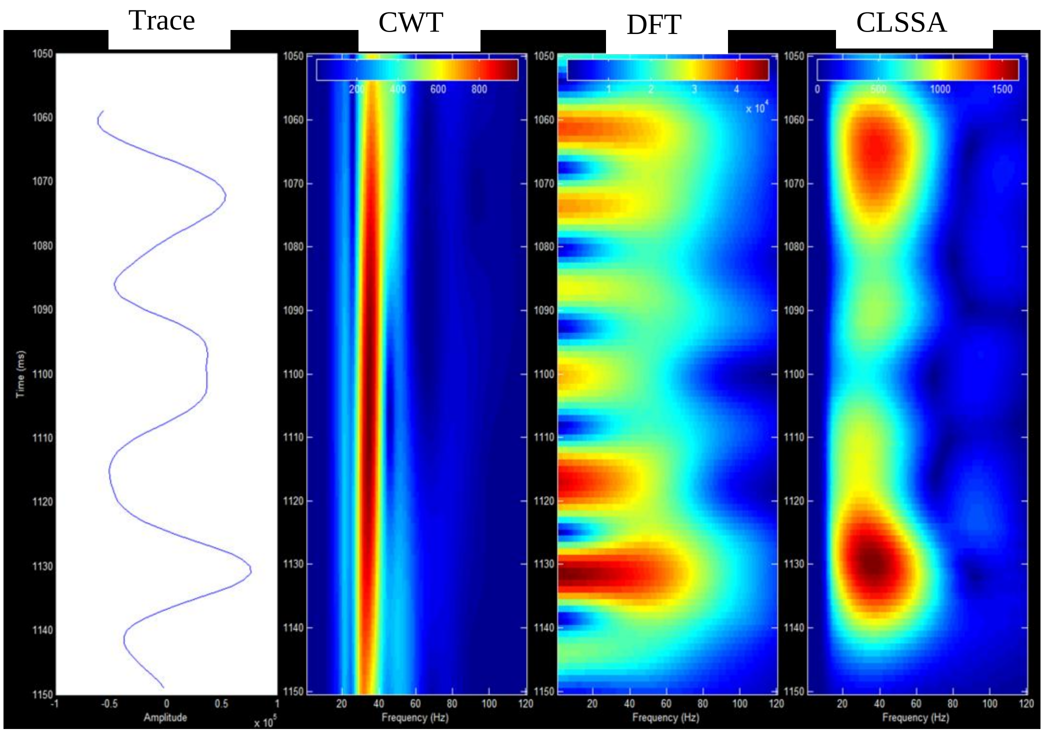

Fig 4.3c: Comparison of frequency gathers for CWT, DFT, and CLSSA with BY18D composite trace using 20ms window

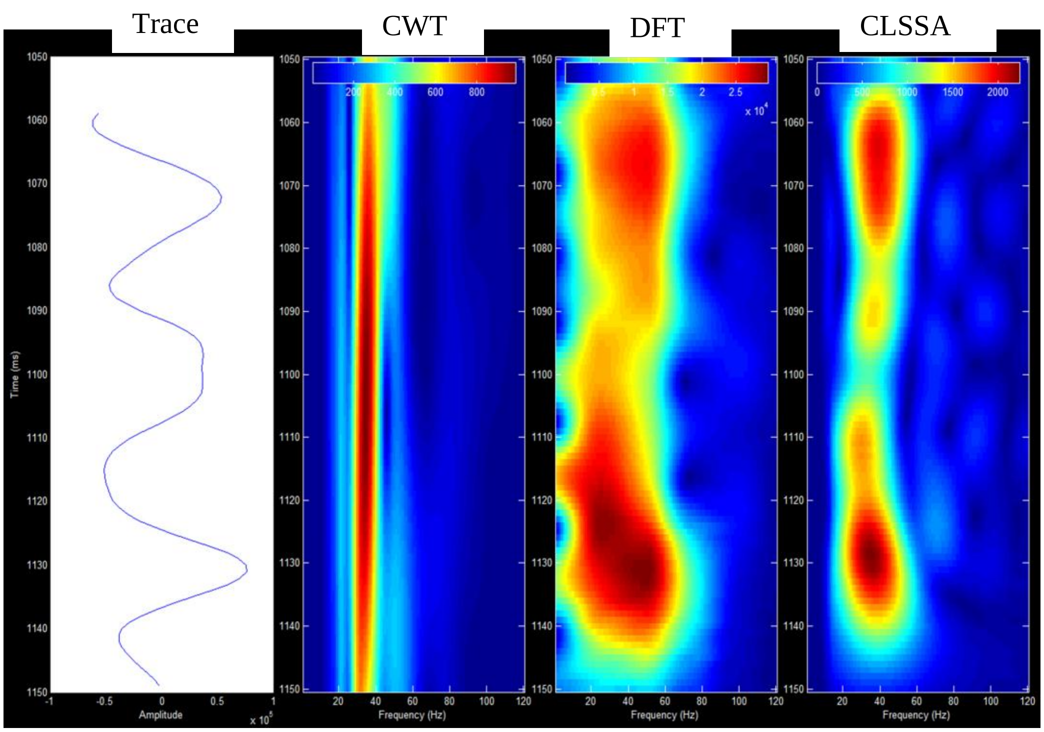

Fig 4.3d: Comparison of frequency gathers for CWT, DFT, and CLSSA with BY18D composite trace using 40ms window

4.3 SPECTRAL INVERSION PROCESS (QUALITY-CONTROLLING)

Spectral inversion, a novel means of improving seismic temporal resolution by removing wavelet destructive interference effect from seismic data generates a broad-band volume with frequencies up to Nyquist (250Hz). The original seismic volume is densely sampled (1ms) and contains high frequency beyond the seismic bandwidth (up to 125Hz) which can introduce noise in the inversion product. Hence, before inverting the dataset, the input to the inversion algorithm must be bandlimited to the seismic frequency band.

Since seismic data are non-stationary signals, there is need to quality-control the time-varying wavelet that drives the inversion process. The extraction of the wavelet that best characterize the seismic response as well as the stabilization factor of the inversion are also important (Chopra et al., 2006b). Despite the notion that the inversion process does not require an apriori model, it is expedient to check the stability of the time-varying wavelet. This can be achieved by convolving the reflectivity series from well with an extracted wavelet and comparing with a composite trace extracted within the vicinity of the well. If there are significant mismatches (misties), parameters for generating the inverted trace are varied until a satisfactory match is derived between the synthetic (well) and composite traces from inverted broad-band seismic (fig 4.4).

The upshot of the wavelet characterization process is a stabilization factor that produces most stable result, least noise and best well-tie. This parameter is now used to drive the spectral inversion process throughout whole survey within the preselected time window for the wavelet extraction (Rodriguez, 2009).

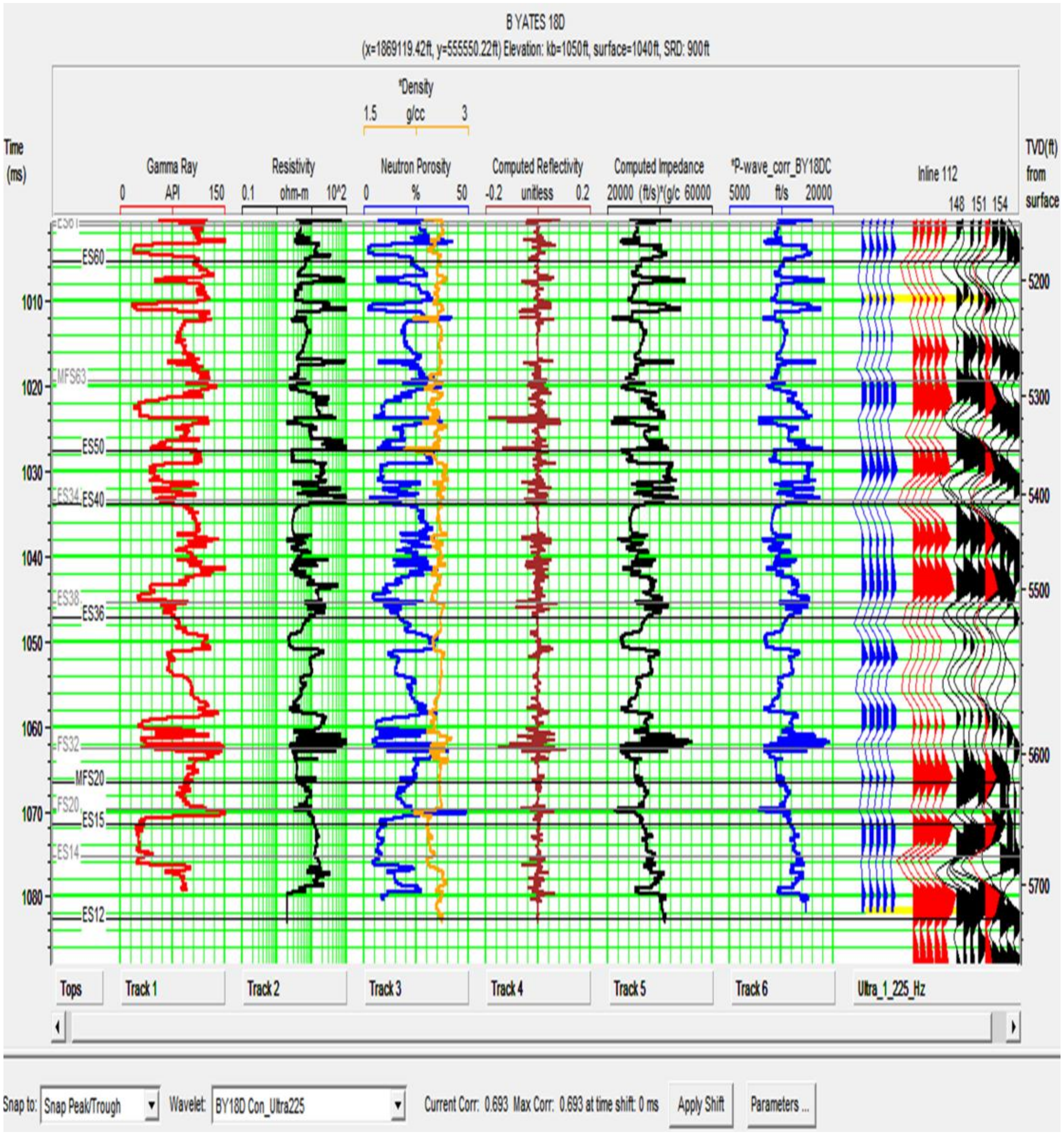

Statistical wavelet (time)

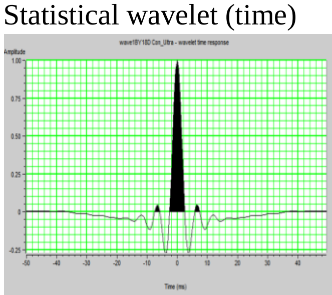

Statistical wavelet (frequency)

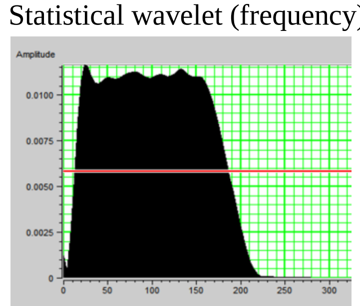

Fig 4.4: Seismic well tie of well BY 18D using inverted volume using well By18D (Correlation coefficient = 0.693)

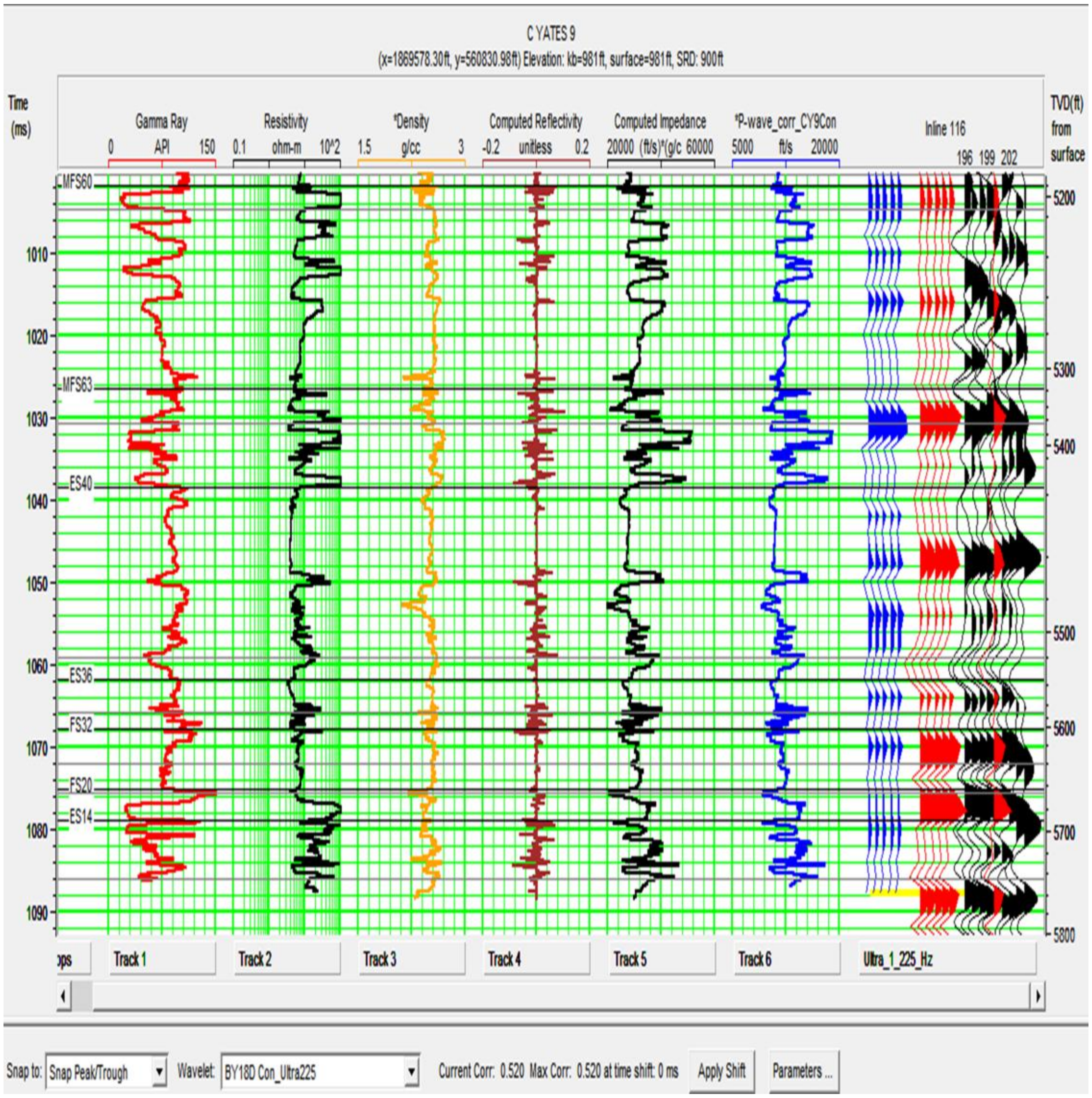

Statistical wavelet (time)

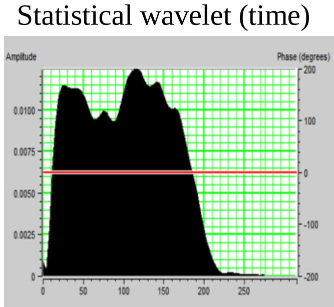

Statistical wavelet (frequency)

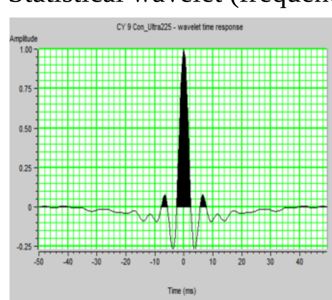

Fig 4.5: Seismic well tie of well CY9 using inverted volume using well by CY9 (Correlation coefficient = 0.52)

Since I have an additional well with impedance logs, the broadband inverted volume is also tied to this well. Extra reflection cycles seen on the synthetic seismogram matches events on the composite extracted from trace from the inverted volume, (fig 4.7 and 4.8). This confirms that the process is effective and the extra detail derived from the broad-band inverted volume are hidden geologic information that would be obscured in conventional seismic data.

Another QC method entails band limiting the high-frequency spectral inversion product and the original Boonsville seismic with a band pass filter (5-10-60-80 Hz) to inspect if the process of spectrally inverting the dataset introduces noise. Figures 4.6 and 4.7 show the comparison of the band-limited products from original seismic and broadband inverted data. The flatness of the amplitude spectrum of band-limited inverted data is a result of wavelet interference removal. This confirms that noise is not introduced during the inversion process.

(a)

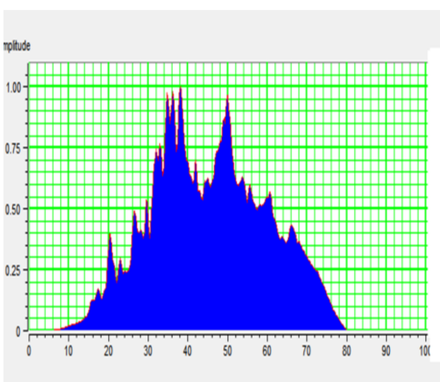

(b)

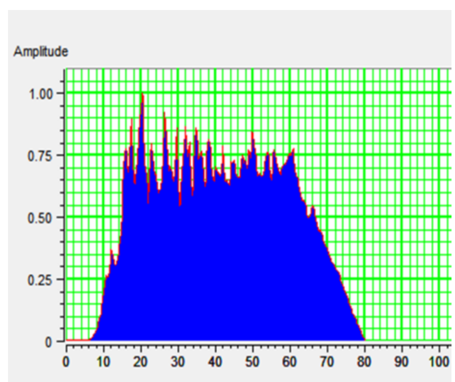

Fig 4.6a: Amplitude spectrum of original seismic after applying band-pass filter

Fig 4.6b: Amplitude spectrum of inverted seismic after applying band-pass filter

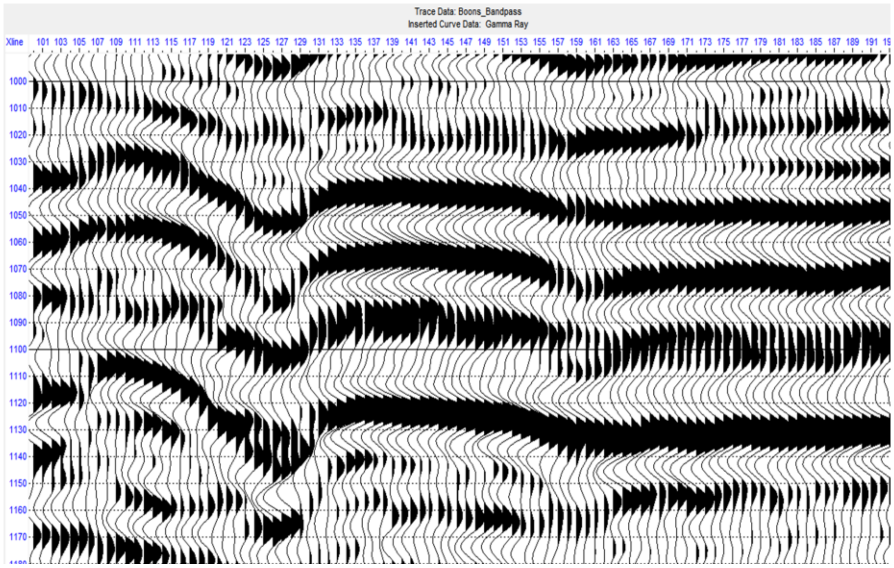

Fig 4.7a: Seismic volume with a band-pass filter (5-10-20-80 Hz)

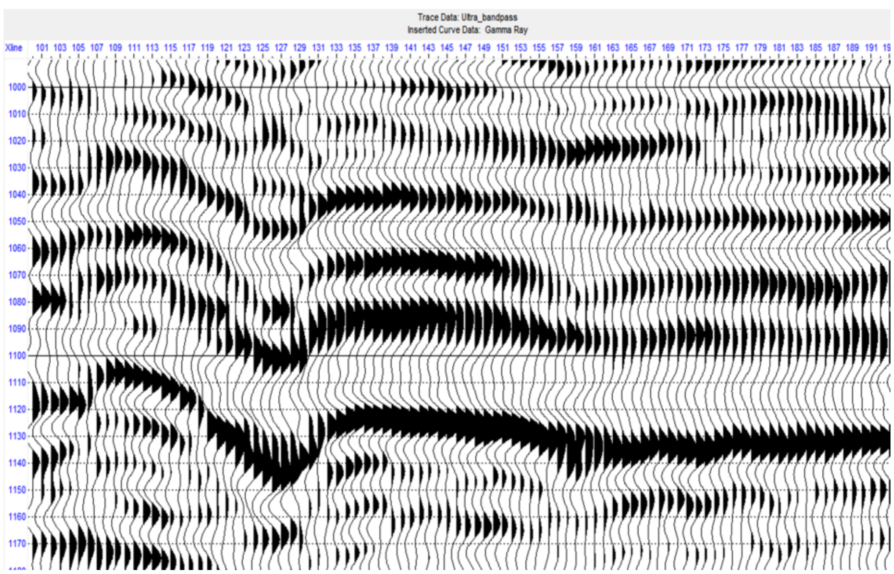

Fig 4.7b: High resolution inverted volume with a band-pass filter (5-10-20-80 Hz)

4.3.1 ANALYSIS OF SPECTRALLY INVERTED DATA

After adequately quality-controlling the inversion process and confirming that the inversion process does not introduce noise and that the extra reflection cycles are upshot of unveiled hidden geologic information, the inverted volume is tied to the wells with the checkshot of original seismic. A statistical wavelet extracted from high frequency spectral inversion volume is convolved with a reflectivity series from the BY18D and CY9 wells. Even though the well ties have lower correlation coefficients (0.692 in BY18D and 0.52 in CY9), the inverted data resolved the top and the base of the sands. Figures 4.8a and 4.8b show the comparison of an arbitrary line taken across BY18D and CY9 wells.

The arbitrary line across the broadband inverted volume shows a significant improvement in temporal resolution in comparison to an equivalent line from conventional seismic. Further inspection of their amplitude spectrum also shows that within the seismic bandwidth (0-100Hz), spectrum of extracted wavelet from spectrally inverted data is flattened; this is due to the removal of wavelet destructive interference effect by the inversion process thereby enhancing vertical resolution.

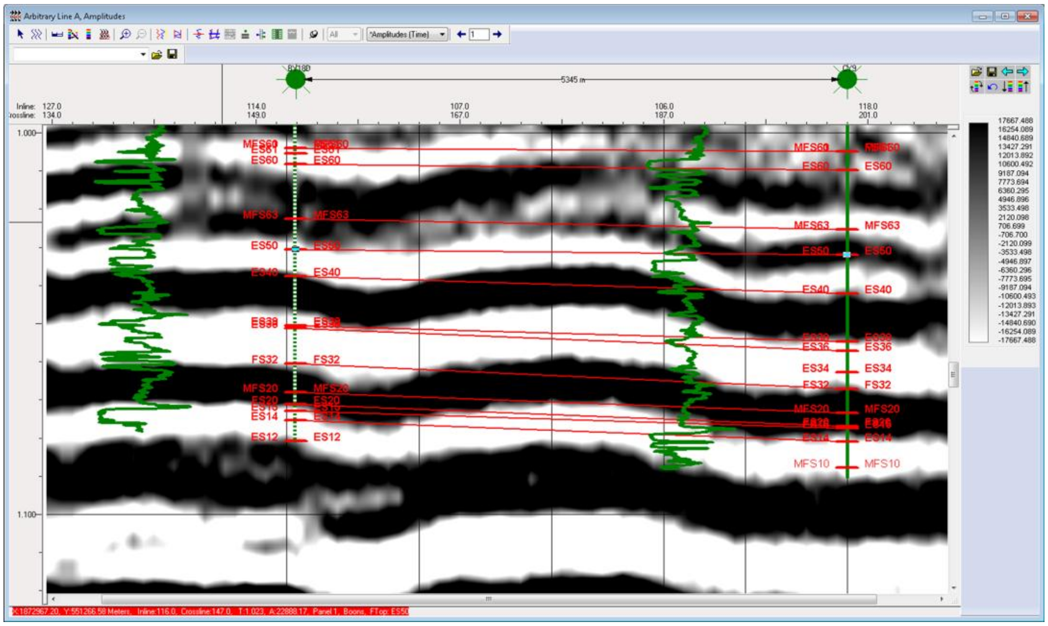

Fig 4.8a: Comparison of original seismic data and inverted volume, top and base of the reservoirs are unresolved.

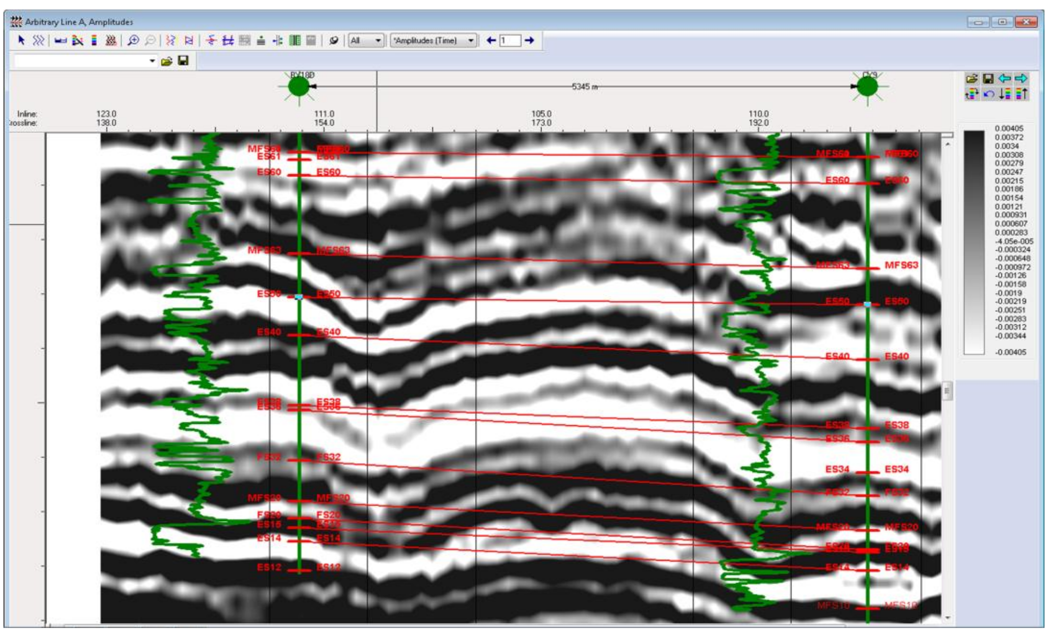

Fig 4.8b: Comparison of original seismic data and inverted volume, top and base of the reservoirs are adequately resolved.

4.3.2 THICKNESS COMPARISON (CROSS-PLOT)

Apparent time thickness is derived from high-resolution spectral inversion volume, since the temporal resolution have been enhanced by the inversion process thereby allowing the delineation of the top and base of reservoirs. True thicknesses are measured from well-logs and cross-plotted against apparent time thickness. The cross-plot yields a correlation coefficient of 0.89. This is highly accurate considering the time thickness used for the analysis is way below seismic resolution (5-10ms).

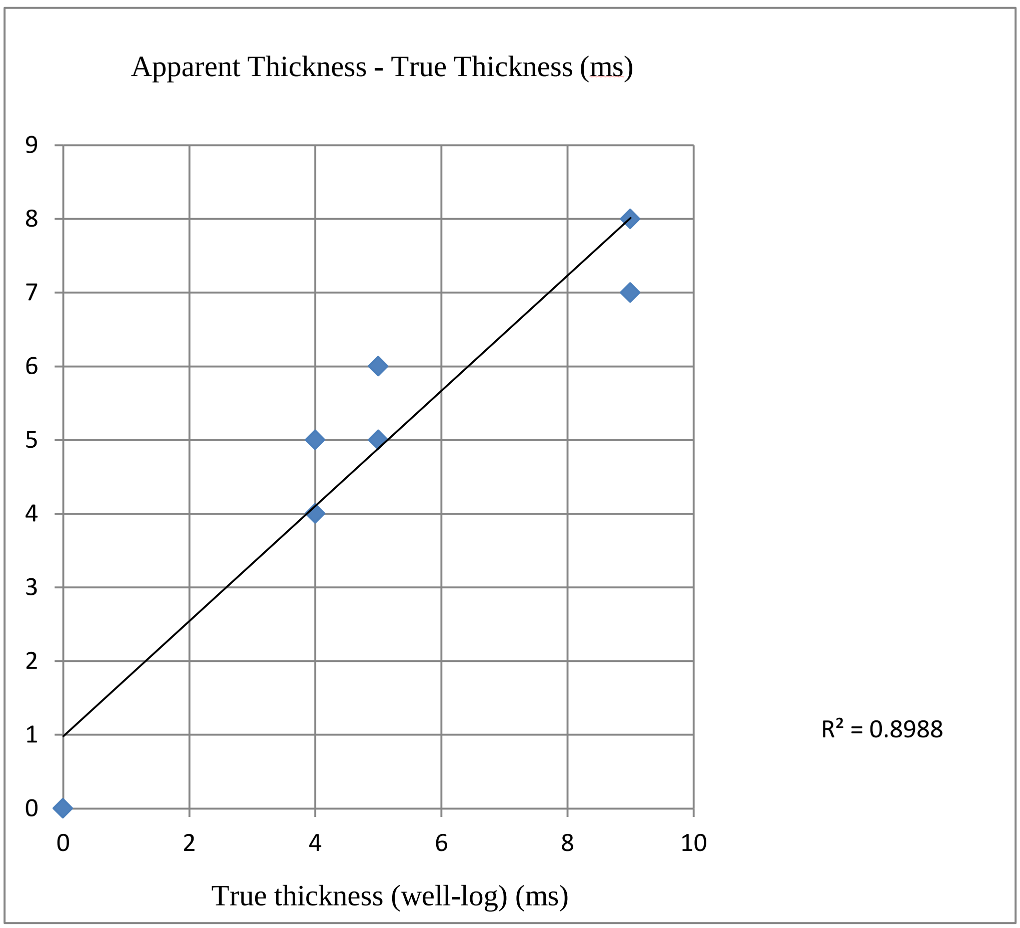

Plot 4.1: Cross-plot of apparent thickness (from inverted seismic) and true thickness (from well-log)

4.3.3 ILLUSIVE STRUCTURAL FEATURES (WAVELET INTERFERENCE)

Spectral inversion is a trace-trace computation without a priori geologic constraint, the inversion technique remove the filtering effect of wavelet on the reflectivity series thereby revealing hidden geologic information in the data. Figure 4.9 below shows the presence of minor faults on the field that were masked on the conventional seismic by the wavelet interference pattern. Furthermore, karst structures observed on vertical seismic section as zones of high signal attenuation (blue circle) are better visualized and continuous on the inverted data. Figures 4.10a and 4.10b is another comparison of inverted and conventional data: the discontuity in bed (indicated by blue arrow) can be misinterpreted to be geologic feature in the conventional seismic whereas on examining an equivalent inverted data, this event is fairly continuous and the discontinuity is as a result of destructive wavelet interference in the original seismic data.

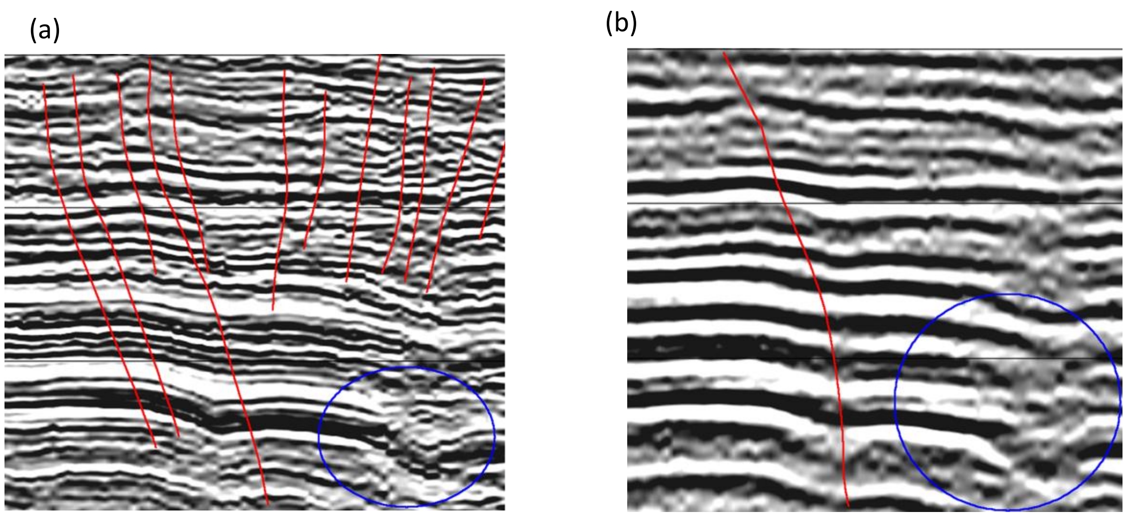

Fig 4.9a: Interpreted Broad-band inverted seismic showing minor fault within the field (red fault sticks) and coherent reflections on the karst structures (blue circle)

Fig 4.9b: Interpreted conventional seismic showing a single minor fault within the field (red fault stick) and attenuated reflections on the karst structures (blue circle)

(A)

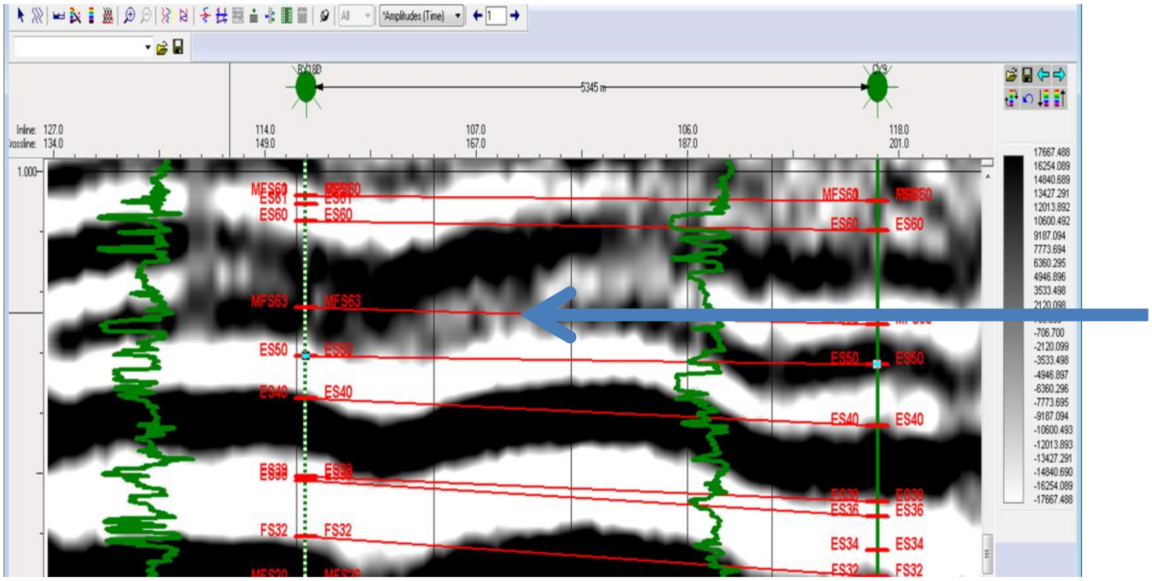

(B)

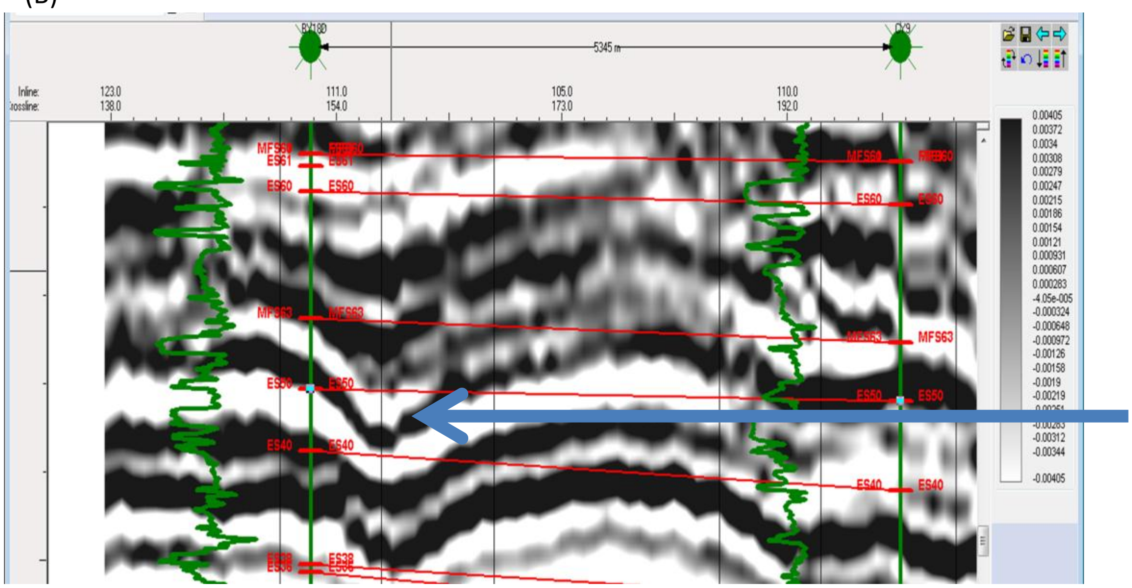

Fig 4.10a: Interpreted conventional seismic, the blue arrow showing a discontinuous event (Correlated ES 50 well-top) due to wavelet distortion

Fig 4.10b: Interpreted Broad-band inverted seismic, the blue arrow showing the continuous reflection (Correlated ES 50 well-top) resolved by removing wavelet distortion.

CHAPTER 5

5.0 CONCLUSIONS

The Atoka Conglomerate is a thin clastic unit of fluvial deltaic origin that forms the producing unit of Boonsville field, North Central, Texas. This clastic unit is characterized by discontinuous and thin facies that pose resolution problems using conventional (seismic) means. Constrained least-squares spectral analysis and high resolution spectral inversion techniques are applied to 3D seismic data from this field to overcome the problem of interfering closely spaced reflections that distort seismic images. The CLSSA method is chosen from a suite of spectral decomposition techniques such as CWT, DFT because it is found to have superior time-frequency resolution.

High resolution spectral inversion method without a priori constraint removes wavelet interference that is produced from the convolution of a seismic wavelet and reflection coefficient. The products of inversion techniques significantly improve temporal resolution by the distinction of closely spaced events. Based on Boonsville field results, the following conclusions were drawn:

- Initial thin bed analysis from wedge models utilizing the conventional amplitude - thickness delineation workflow of Widess (1973) shows that the limit of bed resolution is 55ft (16.7m). In comparison to sand reservoirs in this field whose thickness is less than 40ft (12m), this method fails to procure solution to the prevailing resolution problem.
- Thickness maps generated from mapping coherent reflections on a discrete frequency volume (25Hz) corresponding to tuning thickness produces reasonable results away from well location but highly constrained by well-logs.
- Time-frequency resolution of CLSSA, CWT, and DFT were assessed from computing frequency gathers of traces at varying window lengths, CLSSA shows the best results in

separating individual events. This makes the algorithm ideal for time-frequency decomposition prior to spectral inversion process.

- The spectral inversion method produces a broad-band seismic (with frequencies up to Nyquist) whose extra reflection details unveil subtle geologic features distorted by destructive wavelet interference. The inverted data also enhance lateral continuity of the events and delineate several minor faults that were obscured in the original seismic data by wavelet overprint.
- The cross-plot of apparent thickness (spectral inversion result) and true thickness (from well data) gives a correlation coefficient of 0.89, which is high considering the time thickness used for the computation ranges from 5-10ms. This shows that spectral inversion results are highly correlated with true bed thickness.

These results clearly show that spectral analysis (inversion and decomposition) can be used to resolve bed thicknesses not achievable with conventional Widess resolution. The benefit of improved thickness delineation is the generation of more accurate reservoir models and better stratigraphic interpretation thereby contributing significantly to the success of field exploration and development programs.

REFERENCES

Arya, V. K., and J. Aggarwal, 1982, Deconvolution of seismic data: Benchmark papers in electrical engineering and computer science: volume 24 Hutchinson Ross Publ. Co.

Backus, G.F., 1962, Long-wave elastic anisotropy produced by horizontal layering, JGR, 67, p. 4427-4441.

Burnett, M., J. P. Castagna, E. Méndez Hernández, G. Ziga Rodríguez, L. Figón García, J. Martínez Vázquez, M. Téllez Avilés, and R. Vila Villaseñor, 2003, Application of spectral decomposition to gas basins in Mexico: The Leading Edge, 22, 1130-1134.

Castagna, J.P., S. Sun, and R.W. Siegfried, 2003, Instantaneous spectral analysis: detection of low-frequency shadows associated with hydrocarbons. The Leading Edge, 22, 120-127.

Castagna, J. P., and S. Sun, 2006, Comparison of spectral decomposition methods: First Break, 24, 75-79.

Chakraborty, A., and D. Okaya, 1995, Frequency-time decomposition of seismic data using wavelet-based methods. Geophysics, 60, (6), 1906-1916.

Chung, H., and D. C. Lawton, 1995, Frequency characteristics of seismic reflections from thin beds: Canadian Journal of Exploration Geophysicists, 31, 32–37.

Cohen, L., 1995, Time-frequency analysis: Prentice Hall, Inc.

Chopra, S., J.P. Castagna, and O. Portniaguine, 2006a, Seismic resolution and thin-bed reflectivity inversion. CSEG Recorder, 31, 19-25.

Chopra, S., J.P. Castagna and O. Portniaguine, 2006b, Thin-bed reflectivity inversion SEG/New Orleans 2006 Annual Meeting Expanded Abstract, 2057-2061.

Chopra, S., J.P. Castagna., Yong Xu and Rainer Tonn, 2007, Thin-bed reflectivity inversion and seismic interpretation. SEG/San Antonio 2007 Annual Meeting Expanded Abstract, 1923-1927.

Claerbout, J. F., 1976, Fundamentals of geophysical data processing: Blackwell Scientific Publications.

Craig, A., 1992, AVO analysis of VSP and well log data: CREWES Research Report Vol 4.

Fahmy, W. A., G. Matteucci, D. Butters, and J. Zhang, 2005, Successful application of spectral decomposition technology toward drilling of a key offshore development well: 75th Annual International Meeting of the Society of Exploration Geophysicists, Expanded Abstracts, 262-264.

Gary, F.M., 2003, Numerical methods of Exploration Seismology with algorithms in Matlab: The University of Calgary.

Hardage, B. A., 1996, Boonsville 3-D data set: The leading edge, 15, 835-837.

Hardage, B. A., Simmons, J. L., Lancaster, D. E., Elphick, R. Y., Edson, R. D., and Carr, D. L., 1996, Boonsville 3-D seismic data set: The University of Texas at Austin, Bureau of Economic Geology.

Hlawatsch, F., and G. F. Boudreaux-Bartels, 1992, Linear and quadratic time-frequency signal representations: IEEE Signal Processing, 9, no. 2, 21–67.

Jochen, R.M., J. P. Castagna, and F.S. Floris, 2004, spectral variance in comparison with conventional spectral decomposition attributes: SEG Technical Expanded Abstracts 2004: pp. 441-444.

Lackoff, M., and L. LeBlanc, 1975, Frequency-domain seismic deconvolution filtering: J. Acoust. Soc. Am., 57, 151-159.

Levin, F.K., 1979, Seismic velocities in transversely isotropic media. Geophysics., 44, 918–936.

Liner, C., and F. Tong, 2007, The Backus number: The Leading Edge Apr 2007 26(4), pp. 420-426

Liu, J., and K. J. Marfurt, 2007, Instantaneous spectral attributes to detect channels: Geophysics, 72, no. 2, P23–P31, doi: 10.1190/1.2428268.

Liu, O.Y., 1987, The sources of errors in slowness measurements and an evaluation of full waveform compensation techniques: Soc. Petr. Eng. 62nd Annual Tech. Conf. & Exhib. http://dx.doi.org/ 10.2118/16772-MS.

Marfurt, K. J., and R. L. Kirlin, 2001, Narrow-band spectral analysis and thin-bed tuning: Geophysics, 66, 1274–1283.

Mavko, G., J. Dvorkin., and T. Mukerji, 2009, The Rock Physics Handbook, Cambridge University Press.

Paillet, F.L., and C.H. Cheng, 1991, Acoustic waves in boreholes: CRC Press, Inc.

Partyka, G.A., Gridley, J. and J.A. Lopez, 1997, Processing and interpretational aspect of spectral decomposition. SEG Expanded Abstract, 16, 1055-1058.

Partyka, G.A., Gridley, J. and J.A. Lopez, 1999, Interpretational applications of spectral decomposition in reservoir characterization. The Leading Edge, 18, 353-360.

Partyka G., 2001, Seismic thickness estimation: three Approaches, Pros and Cons. 71th Annual International Meeting, SEG, Expanded Abstracts p. 503-506.

Portniaguine, O., and M. S. Zhdanov, 1999, Focusing geophysical inversion images: Geophysics, 64, 874–887, doi: 10.1190/1.1444596.

Puryear, C.I., and J.P. Castagna, 2008, Layer-thickness determination and stratigraphic interpretation using spectral inversion: theory and application. Geophysics, 73, R37-R48

Puryear, C.I., O. Portniaguine., C.M Cobos ., and J.P. Castagna, 2012, Constrained least-squares spectral analysis: application to seismic data. Geophysics, 77, V143-V167

Rodriguez, J.M., 2009, Spectral decomposition and inversion: case study of a production area in the Cook inlet basin, Alaska, USA : M.S. thesis, University of Houston.

Sinha, S., P. Routh, P. Anno, and J. P. Castagna, 2005, Spectral decomposition of seismic data with continuous-wavelet transform: Geophysics, 70, 19-25.

Souder, W.W., and G.R. Pickett, 1972, A computerized method for the zonation of digitized well-logs. Paper SPE 4012 presented at the Fall Meeting of Society of Petroleum Engineers of AIME, San Antonio, Texas, USA 8-11 October. http://dx.doi.org/10.2118/4019-MS.

Stewart, R.R., P.D. Huddleston., and T.K. Kan, 1984, Seismic versus sonic velocities: A vertical seismic profiling study: Geophysics, 49, 1153-1168.

Taner, M.T., F. Koehler, and R.E. Sheriff, 1979, Complex seismic trace analysis: Geophysics, 44, 1041-1063.

Tirado, S., 2004, Sand thickness estimation using spectral decomposition: M.S. thesis, University of Oklahoma.

Thompson, D. M., 1982, Atoka Group (Lower to Middle Pennsylvanian), Northern Fort Worth Basin, Texas: terrigenous depositional systems, diagenesis, and reservoir distribution and quality: The University of Texas at Austin, Bureau of Economic Geology Report of Investigations No. 125.

Torrence, C., and G. P. Compo, 1998, A practical guide to wavelet analysis: Bulletin of the American Meteorological Society, 79(1), 61–78.

Webster, G., 1978, Deconvolution: geophysics reprints, Soc. Expl. Geophys., vol 1.

Widess, M. B., 1973, How thin is a thin bed: Geophysics, 38, 1176-1180.

Yilmaz, Ö., 2001, Seismic data analysis: SEG Investigations in Geophysics No. 10.